Geophys. J. Int. (2008) **174,** 825–841 doi: 10.1111/j.1365-246X.2008.03836.x

Toward a minimum change model for recent plate motions: calibrating seafloor spreading rates for outward displacement

C. DeMets[1] and D. S. Wilson[2]

[1] *Geology and Geophysics, University of Wisconsin-Madison, Madison, WI* 53706*, USA. E-mail: chuck@geology.wisc.edu*
[2] *Department of Earth Science and Marine Science Inst. University of California-Santa Barbara, Santa Barbara,* CA 93106*, USA*

Accepted 2008 April 28. Received 2008 March 14; in original form 2007 September 1

SUMMARY

We use seafloor spreading distances derived from reconstructions of more than 7000 crossings of young magnetic anomalies along seven plate boundaries to study outward displacement, a source of systematic bias in estimates of seafloor spreading rates, which is caused by a combination of processes that shift magnetic polarity transition zones away from their idealized locations. Linear regressions of 81 independent sequences of seafloor opening distances as a function of their magnetic reversal ages for anomalies younger than C3n.1 (4.19 Ma) yield 75 positively valued intercepts for zero seafloor age, confirming the ubiquitous outward shift of magnetic reversals reported by previous authors. Grouping these data into 29 locally consistent clusters yields better constrained zero-age intercepts that are uniformly positive and average 2.2 ± 0.3 km globally. These values, which are 1–3 km at most locations and are significantly larger (3–5 km) along the well-surveyed Reykjanes and Carlsberg ridges, agree well with published magnetic polarity zone transition widths, which are estimated directly from near-bottom seafloor magnetic measurements. Significant variations in outward displacement along the Southeast Indian Ridge are strongly correlated with changes in axial morphology and axial depth; however, a similar correlation is not observed along other ridges. Forward magnetic anomaly modelling suggests that variations in outward displacement can be explained by differences in the magnetic source layers that are assumed to characterize different spreading centres. If not corrected for outward displacement, the implied systematic upward biases in seafloor spreading rates, which are averaged over the width of Anomaly 1—the youngest reversal that is used for plate reconstructions—range from 6 mm yr^{-1} along the Reykjanes Ridge, where outward displacement is 4–5 km, to 3 mm yr^{-1} along ridges where outward displacement approximates the global average of 2 km.

Key words: Plate motions; Marine magnetics and palaeomagnetics; Mid-ocean ridge processes.

1 INTRODUCTION

Following the discovery that lineated magnetic anomalies in the ocean basins record seafloor spreading along the mid-ocean ridges (Vine & Matthews 1963), a multidecade-long international effort to map, in more detail, the mid-ocean ridge system and its associated magnetic lineations has greatly increased the data that are available for estimating recent and past plate motions. As the precisions of plate motion models that are derived from these data have improved, such models have become increasingly useful for identifying and exploiting apparent changes in plate motions to better understand the timing and nature of changes in plate driving forces. The proliferation of Global Positioning System (GPS) receivers to most areas of the globe since the 1990s has also yielded increasingly precise and complete estimates of instantaneous plate velocities (e.g. Larson *et al.* 1997; Sella *et al.* 2002; Kreemer *et al.* 2003), thereby setting the stage for detecting changes in plate motions up to the present day.

An important consideration for any attempt to detect differences between geological and geodetic plate motion estimates is the degree to which possible systematic errors in one or both types of plate motion estimates might lead to false conclusions about possible recent changes in the plate motions. The potential sources of such errors are numerous. For example, the slip directions of strike-slip earthquakes along transform faults (Argus *et al.* 1989; DeMets 1993) and shallow-thrust earthquakes from obliquely convergent subduction zones (Jarrard 1986; McCaffrey 1992) are biased relative to independent measures of plate slip directions across those features and thus degrade plate motion estimates derived from such observations. Similarly, zones of slow deformation such as rifting

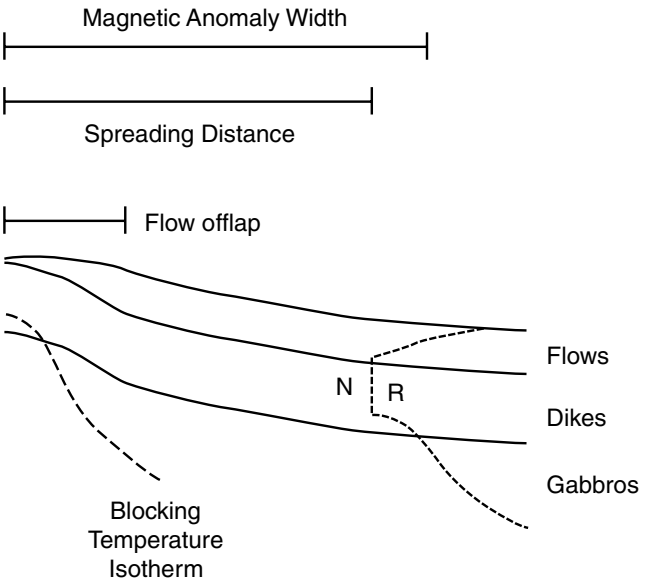

Figure 1. Schematic cross-section of the magnetic structure of upper oceanic crust near the ridge axis, simplified from Kidd (1977). Lava flows acquire magnetization over a range of distances by accumulating away from the axis. Gabbros magnetize over a range of distances by cooling through a sloping blocking-temperature isotherm (at which magnetization becomes stable over geologiccal time). The width of the youngest magnetic polarity zone predicted by this model is greater than the spreading distance since the last magnetic reversal. In most cases, this outward displacement of the polarity boundaries, summed over both plates, will be similar to the transition width of a single polarity boundary.

in eastern Africa (Chu & Gordon 1999; Royer *et al.* 2006) and motion of the Baja California peninsula relative to the Pacific plate (Dixon *et al.* 2000; Plattner *et al.* 2007), which are not explicitly modelled in the RM2 or NUVEL-1 global plate motion models (Minster & Jordan 1978; DeMets *et al.* 1990), introduce biases into both models. Finally, GPS station velocities that are used to estimate instantaneous plate motions are also subject to systematic biases, particularly due to problems with the terrestrially-based geodetic reference frames, relative to which geodetic station velocities are specified (Argus *et al.* 1999; Blewitt 2003; Argus 2007).

An additional source of systematic error stems from the phenomenon of outward displacement (Fig. 1), the subject of this paper. Outward displacement is caused by a variety of processes that collectively widen the zone within which magnetic field reversals are recorded in new oceanic crust (Atwater & Mudie 1973). These processes include extrusion of new magma onto adjacent older crust of opposite magnetization, intrusion of dykes into adjacent older crust of opposite magnetization and the accumulation of magnetized gabbros at the base of the crust, which gives rise to outward sloping reversal boundaries and extensional faulting of magnetic reversal boundaries (Sempere *et al.* 1987). All of these preferentially affect older crust adjacent to the spreading axis, and hence shift the midpoint of a magnetic polarity transition zone away from the spreading axis (Fig. 1). Consequently, seafloor spreading rates that are determined by reconstructing magnetic lineations from opposite sides of a spreading centre are systematically faster than the true spreading rate.

Numerous near-bottom marine magnetic profiles that have been inverted to solve for the magnetization distribution of the seafloor, exhibit widths for individual magnetic polarity transition zones that range from 1 to 5 km for a wide range of seafloor spreading rates (10–150 mm yr^{-1}), with most estimates clustered around 2 km (e.g. Atwater & Mudie 1973; Klitgord *et al.* 1975; Macdonald *et al.* 1980, 1983; Sempere *et al.* 1987, 1990; Tivey *et al.* 1998). Given that the crossover point between seafloor of opposite magnetization is located approximately midway through a polarity transition zone (Macdonald *et al.* 1983), average transition zone widths of 2 km imply that individual polarity reversals are displaced outwards from the axis of seafloor spreading by ∼1 km relative to their idealized locations. By implication, the total outward displacement between two same-age magnetic reversals that flank a seafloor spreading centre is 2 km. The ∼3 mm yr^{-1} implied bias in seafloor spreading rates that are determined from the width of Anomaly 1 (0.781 Ma) exceeds the prediction uncertainties in most published plate motion models.

Herein, we undertake an independent, kinematically-based test for the existence and magnitude of outward displacement, with a primary goal of estimating a correction for future models of plate motions that are derived from marine magnetic data. Our analysis is based on the simple principle that a linear regression of a sequence of seafloor opening distances from a spreading centre whose motion has remained constant for the past few Myr or longer should yield a positive distance-axis intercept for zero-age seafloor if the midpoints of magnetic polarity transition zones are displaced systematically outward from their idealized reversal locations. Our analysis is limited to magnetic reversals younger than 5 Ma. This not only reduces the possibility of sampling a change in plate motion that would violate the constant-motion requirement implicit in our analysis but limits our analysis to magnetic reversals whose ages are well determined from astrochronological dating (Lourens *et al.* 2004).

The paper is organized as follows. Following a brief description of the data and methods, we derive distance-axis intercepts at zero seafloor age from regressions of 81 independent age-distance sequences from the mid-ocean ridge system (Fig. 2), each determined from reconstructions of anomaly crossings that we identified for one or several well-surveyed seafloor spreading segments. We find that 95 per cent of the intercept values are positive, indicating that magnetic polarity transition zones are shifted outwards from their idealized locations. We then estimate intercept values from 29 age-distance sequences that we derived from the same anomaly crossings but consolidated into larger data subsets to reduce the magnitude of the underlying random errors. This yields positive-valued zero-age intercepts for all 29 age-distance sequences, ranging from 0 to 5.5 km and averaging 2.2 ± 0.3 km, in excellent accord with estimates of outward displacement implied by inversions of near-bottom magnetic profiles (Sempere *et al.* 1987). In the latter part of the paper, we describe evidence for regionally significant differences in outward displacement, particularly along the Southeast Indian Ridge, where the magnitude of outward displacement is strongly correlated with axial morphology and axial depth. In the absence of any similar correlation along other seafloor spreading centres, we examine the hypothesis that differences between the magnetic source layers are responsible for variations in outward displacement we observe along the Southeast Indian Ridge and Reykjanes Ridge. We find that forward modelling of the magnetic anomalies at both locations, assuming plausible magnetic source layer geometries and characteristics, can reproduce the observed factor-of-two change in outward displacement across the eastern edge of the Australia–Antarctic discordance and unusually wide outward displacement along the Reykjanes Ridge.

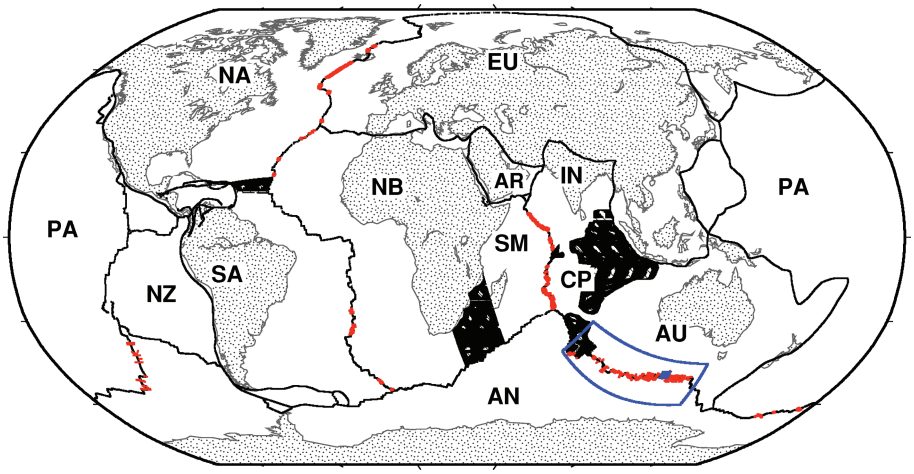

Figure 2. Locations of all anomaly crossings (red circles) used to estimate long-term seafloor spreading rates and outward displacement. The blue dashed line and blue square outline the regions covered by Figs 9 and 12, respectively. Plate abbreviations: AN, Antarctic; AR, Arabian; AU, Australian; CP, Capricorn; EU, Eurasian; IN, Indian; NA, North American; NB, Nubian; NZ, Nazca; PA, Pacific; SA, South American and SM, Somalian.

2 DATA AND METHODS

2.1 Magnetic data

Our kinematic analysis is based on reconstructions of ∼7100 crossings of magnetic reversals C1n(o) (0.781 Ma) through C3n.1 (4.187 Ma) (Table 1) from seven plate boundaries along which seafloor spreading rates appear to have remained constant or nearly constant for the past 3–5 Myr. Six of the seven plate boundaries are located in the Atlantic and Indian Ocean basins (Fig. 2) and one in the Pacific basin. We have previously employed subsets of these anomaly crossings to study recent plate kinematics along the southern Mid-Atlantic Ridge (Weiland *et al.* 1995), the Central Indian Ridge (DeMets *et al.* 2005), the Carlsberg Ridge (Merkouriev & DeMets 2006) and the Kolbeinsey, Reykjanes and northern Mid-Atlantic ridges (Merkouriev & DeMets 2008).

We extracted all of the anomaly crossings from original shipboard magnetic and aeromagnetic data that we compiled from the National Geophysical Data Center and a variety of foreign sources. Many of the data are drawn from densely surveyed areas of the mid-ocean ridges, where numerous crossings of the magnetic reversals help to identify and avoid seafloor features such as small ridge offsets and pseudo-faults that disrupt magnetic anomaly sequences. Best-fitting reconstructions of the anomaly crossings for the individual study areas are determined using techniques that are described in the following section. The uncertainties we assign to the locations of individual anomaly crossings range from ±0.7 to ±2.0 km and are based on the dispersion of the anomaly crossings with respect to their best-fitting reconstructions.

Table 1. Assumed pole locations and best-fitting angular rotation rates.

Plate pair	Lat. °N	Long. °E	ω (°Myr)	DOF	χ^2
AN–PA[1]	65.1	−80.9	0.858	280	183.3
AU–AN[1]	11.2	41.8	0.636	756	588.2
CP–SM[2]	11.8	49.3	0.638	588	567.9
EU–NA[3]	62.8	137.9	0.2065	2058	1709.3
IN–SM[4]	21.9	30.7	0.394	1272	1234.4
NB–NA[5]	78.8	38.3	0.2285	378	335.5
NB–SA[1]	58.3	−38.7	0.292	483	404.4

DOF is degrees of freedom, which equals the total anomaly crossings inverted for the plate pair adjusted for the parameters that are estimated, which consist here of the rate of angular rotation, two parameters for each spreading segment being reconstructed along the boundary and separate values of outward displacement for each study area along the plate boundary. The rotation rate uncertainty is determined using a suitable *F*-ratio test and accounts for the added uncertainty from estimating multiple values of outward displacement per plate pair. Sense of rotation is counter-clockwise for the first plate relative to the fixed second plate. Assumed pole locations are from the following sources: (1) this study; (2) DeMets *et al.* (2005), best average pole for present to Chron 4n.2; (3) Merkouriev & DeMets (2008); (4) Merkouriev & DeMets (2006), best average pole for present to Chron 4A and (5) DeMets *et al.* (1990).

Most Pacific basin seafloor spreading centres are excluded from our analysis due to abundant evidence for changes in Pacific basin plate motions over the past few million years. Fig. 3 summarizes opening distances since 5.5 Ma for a variety of plate pairs after subtracting from each the contribution of steady spreading. In contrast to the opening distance time-series for the Pacific–Antarctic and Australia–Antarctic plate boundaries (upper two sequences in Fig. 3), which are consistent with constant seafloor spreading rates and have zero-age intercepts of 1–2 km, all three spreading distance time-series for the Cocos and Nazca plate boundaries (lower three sequences in Fig. 3) show evidence for significant changes in motion at ∼1.5–1 Ma, with zero-age intercepts that are in some cases significantly negative (Fig. 3) and in most cases vary significantly with location along a given plate boundary (not shown).

These recent Pacific basin motion changes are also described in the literature. Naar & Hey (1989) find a Nazca–Pacific pole for C1n(o) that describes slower spreading rates and a steeper rate gradient than predicted by the C2A pole of DeMets *et al.* (1994), in accord with results shown in Fig. 3. Along the Pacific–Cocos plate boundary. DeMets & Wilson (1997) find that the spreading rate gradient decreased from C2An to C1n(o), consistent with a change in pole location and also consistent with evidence for a counter-clockwise change in the Cocos–Pacific direction of motion at about 1 Ma indicated by swath mapping data (Macdonald *et al.* 1992). Along the Cocos–Nazca boundary, Wilson & Hey (1995) find a different gradient in spreading rates since 0.78 Ma than for older magnetic anomalies and conclude that the location of the rotation pole changed at 1.5 Ma. Along the Chile Rise, Tebbens *et al.* (1997) determine a full spreading rate of 53 mm yr^{-1} over the past 0.78 Ma, slower than the 62 mm yr^{-1} average rate they determined

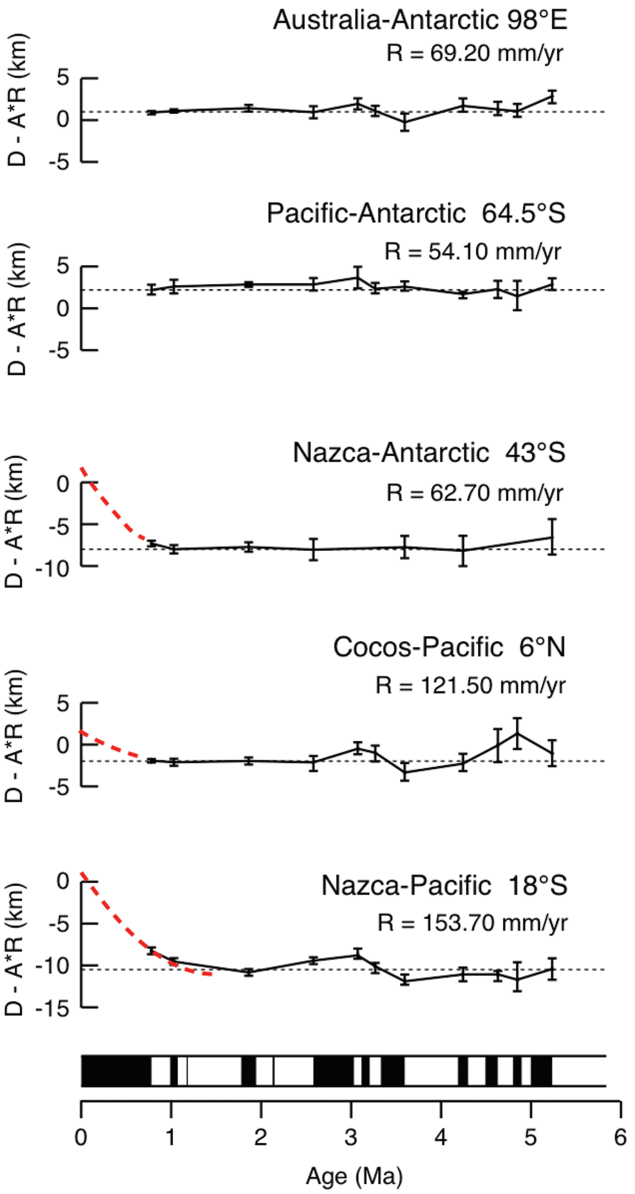

Figure 3. Reduced spreading distance as a function of age for two plate pairs without strong evidence for recent motion changes (top two panels) and three plate pairs with probable motion changes at 1–1.5 Ma (bottom three panels). Reduced distance is defined as the full spreading distance D minus the product of the anomaly age A and reduction rate R. Dotted lines indicate constant spreading at the reduction rate and red dashed lines show interpreted recent changes in motion based on constraints imposed by a zero-seafloor-age intercept, which is slightly positive (corresponding to positive outward displacement). Most profiles are updated from Wilson (1993a) or Krijgsman *et al.* (1999). The sometimes large negative intercepts and variations in the value of the zero-age intercept with location along the plate boundary (described in the text) for the Nazca and Cocos plate pairs can only reasonably be explained by recent plate motion changes, rendering these pairs relatively useless for estimating outward displacement.

for rates between 5 Ma and 1 Ma and consistent with the large negative (−8 km) opening distance deficit we find at present with respect to that projected from the spreading rate from 5 Ma to 1 Ma (middle sequence in Fig. 3).

Numerous marine magnetic data from the well surveyed Pacific–Rivera and Pacific–Juan de Fuca plate boundaries indicate that their motions relative to the Pacific plate have also changed significantly since 3 Ma (Wilson 1993b; DeMets & Traylen 2000). The available evidence thus indicates that changes in seafloor spreading rates have occurred along all but one of the Pacific basin seafloor spreading centres within the time period covered by this study, making these spreading centres unsuitable for our work. In addition, we are also unable to use data from the well-surveyed Southwest Indian Ridge because the seafloor spreading magnetic anomaly sequence along this slow spreading centre is too poorly expressed to yield the detailed reconstructions that are required for our analysis.

2.2 Determination of best-fitting opening distances

Fig. 4 illustrates the methods we use to determine seafloor spreading distances and outward displacement, using as an example anomaly

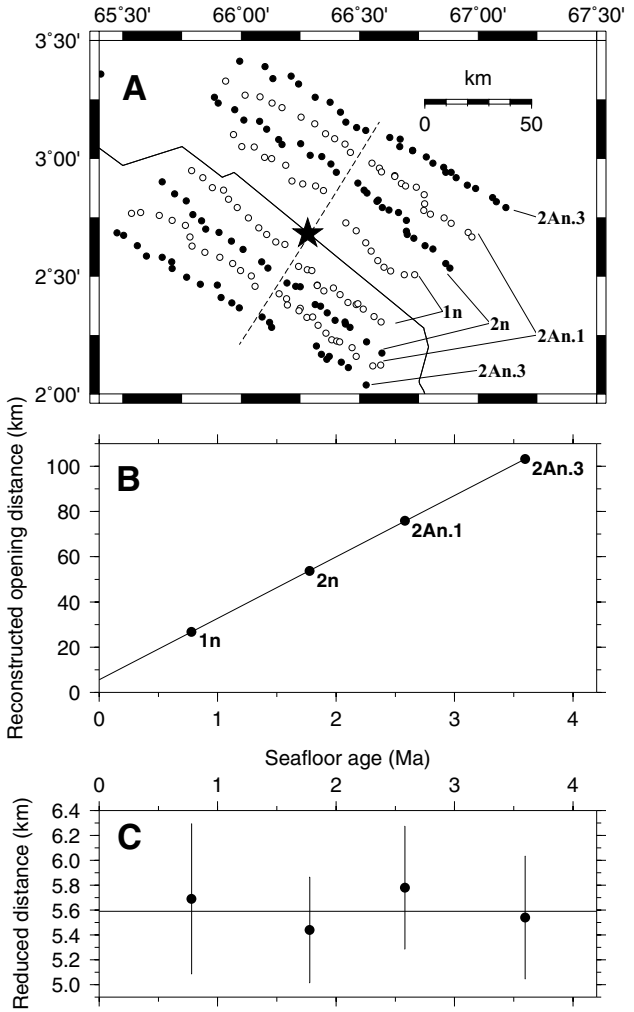

Figure 4. (a) Example of magnetic anomaly crossings employed to estimate total opening distances for magnetic reversals 1n, 2n, 2An.1 and 2An.3. The magnetic anomaly crossings are taken from a study of Carlsberg Ridge seafloor spreading (Merkouriev & DeMets 2006). Star indicates geographic centroid of the anomaly crossings. (b) Best weighted linear fit to opening distances determined from reconstructions of anomaly crossings shown in panel (a). Distances are estimated along the dashed flow line shown in panel (a). Opening distance uncertainties are smaller than the symbols. The best-fitting line has a value of 5.6 km for zero-age seafloor, representing a kinematic estimate of outward displacement. (c) Reduced distances after subtracting the product of the reversal age and best-fitting rate from panel (b). Vertical scale is expanded to show the best-fit intercept of 5.6 km and opening distance uncertainties. Average misfit is 150 m.

crossings from a well-surveyed segment of the Carlsberg Ridge (Merkouriev & DeMets 2006). For an assumed opening pole located at 21.9°N, 30.7°E (Merkouriev & DeMets 2006), we use standard techniques to invert crossings of the old edge of Anomaly 1, the young edge of Anomaly 2 and the old and young edges of Anomaly 2A to identify their best-fitting rotation angles (Hellinger 1979; Royer & Chang 1991). We next derive total seafloor opening distances and their uncertainties (Fig. 4b) along a centrally located flow line (shown by the dashed small circle in Fig. 4a) from the opening pole and best opening angles. The small opening distance uncertainties, which average only ±0.5 km, permit a strong test for the steadiness of post-4 Ma opening rates and for a non-zero distance-axis intercept.

We estimate the slope and zero-age intercept that best fit the age-distance sequence shown in Fig. 4(b) from a weighted linear regression in which the reversal ages are assumed to be known perfectly and the opening distances are weighted by their formal uncertainties. The best-fitting linear model fits each of the opening distances within its estimated uncertainty (Fig. 4c), consistent with our assumption of steady seafloor spreading at this location. The best-fitting line intersects the zero-seafloor-age axis at a distance of 5.6 km (Fig. 4b), consistent with either a significant outward shift of the reversal boundaries with respect to their idealized locations or a spreading rate acceleration after 0.78 Ma.

For each of the seven plate boundaries we studied, we applied the above method to estimate a sequence of well-constrained opening distances for non-overlapping, well-surveyed areas of the plate boundary. We began by dividing the ∼7100 anomaly crossings into 81 non-overlapping study areas (locations shown in Fig. 2), each consisting of one or more well-surveyed spreading segments. The number of anomaly crossings that were used to determine any single opening distance within these 81 regions ranges from as few as three to as many as 110. Per plate boundary, we fixed the location of the opening pole to a pre-determined value (Table 1) to enforce consistent opening directions for all reversals that were reconstructed along that plate boundary.

Our analysis of the 81 age-distance sequences (Section 3.1) yields similar values for outward displacement for many study regions that are adjacent to each other, indicating that the data from some of the study areas can be combined without losing any information about significant variations in outward displacement. We therefore consolidated the ∼7100 anomaly crossings into 29 larger study areas (Table 2) and determined best-fitting opening angles and age-distance sequences for each. These opening distances, which are derived from more anomaly crossings and hence have smaller uncertainties, yield better-determined estimates for outward displacement. Results for both sets of age-distance sequences are described in Sections 3.1 and 3.2.

2.3 Estimation of opening rates and outward displacement subject to a rigid plate constraint

One shortcoming of the above procedure is that the best-fitting opening rates for each study area along a given plate boundary are estimated independently and are therefore not required to vary sinusoidally as a function of angular distance from the pole of opening, as they should if both plates that flank the plate boundary are rigid. As a consequence, useful information is lost about both the long-term opening rates and outward displacement because more parameters are used to fit the data than are necessary.

In Section 3.2, we attempt to capture this lost information by inverting simultaneously all the data from a single plate boundary to estimate its opening history and variations in the magnitude of outward displacement along the plate boundary. We accomplish this as follows: given the crossings of N magnetic reversals from a plate boundary that is subdivided into M non-overlapping regions, the anomaly crossings for all N reversals are inverted simultaneously to determine the rate of angular opening and M location-dependent small-angle corrections (one for each of the pre-defined regions described above) that minimize the cumulative least-squares misfit to all of the data. Within the inverse code, the angular opening rate is converted to an equivalent series of N finite opening angles using the magnetic reversal ages from Table 2, and each of the N opening angles are further adjusted by the M time-independent small angles to compensate for differences in outward displacement within the M pre-defined regions. Regions characterized by smaller or greater outward displacement give rise to local small-angle adjustments that locally decrease or increase the total opening angle to improve the fit in that region. The misfit for each of the N reversals is determined using fitting criteria described by Hellinger (1979).

Following the estimation procedure, the M best-fitting small angles are converted to their equivalent values of outward displacement in units of km, based on the geographic midpoint of each study area. The best-fitting rate of angular opening and estimated values for outward displacement that result from the above procedure satisfy the rigid plate requirement for all magnetic reversals that were included in the inversion.

One advantage of the simultaneous inversion procedure is that information in the data about the angular opening history and outward displacement is propagated effectively between well surveyed and sparsely surveyed areas of the plate boundary. For example, because anomaly crossings from densely surveyed parts of a plate boundary strongly constrain the rate of angular opening everywhere along the plate boundary, estimates of outward displacement can be determined with more confidence in areas of the plate boundary where the magnetic anomaly crossings are too sparse to constrain reliably both the local value for outward displacement and the angular opening rate.

A disadvantage of the above procedure is the trade-off in fit that is introduced between the assumed location of the opening pole and the estimated values of outward displacement. An erroneous pole location or any migration of the pole during the time spanned by the data will result in an incorrect gradient in the amount of opening that is predicted for the plate boundary. The biased pole location precludes obtaining best estimates of outward displacement from the inversion and instead, introduces artefacts in their apparent magnitudes that act to offset the effect of the incorrect pole location. Numerical experiments indicate that our estimates of outward displacement can change by as much as 1–1.5 km for pole locations that are wrong by as little as 1–2 angular degrees. The fixed-pole assumption that we employ thus limits the accuracy of our results. More generally, we note that outward displacement limits the accuracy with which any finite rotation can be determined from marine magnetic data, unless independent information is available about the pole location (such as might be extracted from fracture zone crossings).

3 ESTIMATES OF OUTWARD DISPLACEMENT FROM MARINE MAGNETIC DATA

3.1 Results from 81 local age-distance sequences

Linear regressions of the 81 age-distance sequences that are described in the previous section yield 75 positive-valued,

Table 2. Opening distance time-series.

Correlation	Reversal	An–Pa[1]	An–Pa[2]	An–Pa[3]	Au–An[4]	Au–An[5]	Au–An[6]
point	age (Ma)	64.1°S, 167.3°W	52.3°S, 117.4°W	41.0°S, 111.3°W	45.4°S, 93.1°E	49.5°S, 111.1°E	49.2°S, 125.1°E
C1n(o)	0.781	$45.60^{+0.33}_{-0.33}$ (47)	$65.36^{+0.67}_{-0.57}$ (24)	$72.77^{+0.95}_{-0.95}$ (11)	$54.22^{+0.32}_{-0.21}$ (102)	$57.42^{+0.22}_{-0.33}$ (114)	$57.67^{+0.44}_{-0.45}$ (51)
C1r.1n(c)	1.03	$60.38^{+0.39}_{-0.47}$ (40)	$88.10^{+0.67}_{-0.67}$ (12)	$95.73^{+0.74}_{-0.74}$ (10)	$71.34^{+0.22}_{-0.32}$ (104)	$74.60^{+0.45}_{-0.33}$ (91)	$74.86^{+0.44}_{-0.56}$ (48)
C1r.2n(c)	1.179	$70.14^{+0.60}_{-0.53}$ (15)	$101.48^{+0.67}_{-0.67}$ (11)	$110.69^{+1.37}_{-1.27}$ (3)	—	—	—
C2n(y)	1.778	$101.15^{+0.47}_{-0.52}$ (22)	$148.30^{+0.76}_{-0.76}$ (10)	$164.19^{+0.84}_{-0.85}$ (10)	—	$125.93^{+1.00}_{-0.89}$ (20)	$124.21^{+1.55}_{-1.44}$ (10)
C2n(c)	1.8615	$106.43^{+0.60}_{-0.53}$ (22)	$156.80^{+0.86}_{-0.76}$ (15)	$171.35^{+0.37}_{-0.48}$ (12)	$128.65^{+0.75}_{-0.74}$ (22)	$133.13^{+0.56}_{-0.66}$ (28)	$133.86^{+0.66}_{-0.56}$ (27)
C2n(o)	1.945	$111.84^{+0.47}_{-0.39}$ (28)	$161.10^{+0.86}_{-0.86}$ (9)	$178.51^{+0.73}_{-0.74}$ (11)	—	—	—
C2r.1n(c)	2.138	$21.68^{+0.46}_{-0.47}$ (25)	$177.16^{+0.95}_{-0.96}$ (8)	$194.20^{+0.84}_{-0.74}$ (10)	—	—	—
C2An.1(y)	2.581	$147.08^{+0.46}_{-0.53}$ (24)	$221.97^{+1.01}_{-1.10}$ (5)	$238.01^{+1.05}_{-1.05}$ (12)	$176.92^{+1.07}_{-1.05}$ (14)	$184.24^{+0.55}_{-0.67}$ (40)	$183.43^{+0.66}_{-0.56}$ (27)
C2An.1r(c)	3.074	—	—	—	$211.80^{+1.06}_{-1.17}$ (9)	$219.27^{+0.66}_{-0.67}$ (29)	$216.81^{+1.55}_{-1.44}$ (11)
C2An.2r(c)	3.268	—	—	—	$224.24^{+0.95}_{-0.96}$ (8)	$233.23^{+0.78}_{-0.66}$ (33)	$231.78^{+1.78}_{-1.77}$ (10)
C2An.3(o)	3.596	—	—	—	$246.14^{+1.17}_{-1.28}$ (14)	$256.07^{+0.66}_{-0.67}$ (34)	$254.62^{+1.22}_{-1.33}$ (20)

Correlation	Reversal	Au–An[7]	Cp–Sm[8]	Cp–Sm[9]	Cp–Sm[10]	Cp–Sm[11]	Cp–Sm[12]
Point	Age (Ma)	50.3°S, 131.2°E	10.5°S, 66.4°E	14.7°S, 66.4°E	19.0°S, 65.6°E	21.8°S, 68.9°E	25.1°S, 69.9°E
C1n(o)	0.781	$54.14^{+0.44}_{-0.55}$ (68)	$28.50^{+0.94}_{-0.89}$ (21)	$30.45^{+0.87}_{-0.88}$ (41)	$31.83^{+1.20}_{-1.14}$ (20)	$35.48^{+0.56}_{-0.55}$ (84)	$40.06^{+0.67}_{-0.67}$ (54)
C1r.1n(c)	1.03	$73.40^{+0.55}_{-0.55}$ (46)	—	—	—	—	—
C2n(y)	1.778	$124.13^{+0.99}_{-0.99}$ (24)	—	—	—	—	—
C2n(c)	1.8615	$130.73^{+0.55}_{-0.55}$ (31)	$63.90^{+0.84}_{-0.84}$ (21)	$70.94^{+0.99}_{-0.93}$ (36)	$77.73^{+1.21}_{-1.20}$ (19)	$85.16^{+0.91}_{-0.90}$ (42)	$90.46^{+0.82}_{-0.74}$ (47)
C2An.1(y)	2.581	$180.25^{+0.55}_{-0.55}$ (46)	$87.54^{+0.89}_{-0.84}$ (20)	$98.37^{+0.81}_{-0.81}$ (38)	$105.69^{+1.34}_{-1.33}$ (16)	$116.89^{+0.90}_{-0.90}$ (41)	$124.04^{+0.97}_{-1.04}$ (30)
C2An.1r(c)	3.074	$215.91^{+0.55}_{-0.66}$ (42)	—	—	—	—	—
C2An.2r(c)	3.268	$227.79^{+0.66}_{-0.77}$ (43)	—	—	—	—	—
C2An.3(o)	3.596	$250.68^{+0.66}_{-0.55}$ (41)	$122.62^{+1.00}_{-0.83}$ (18)	$134.80^{+0.87}_{-0.75}$ (41)	$146.27^{+1.40}_{-1.27}$ (15)	$161.35^{+0.91}_{-0.90}$ (36)	$171.69^{+0.97}_{-1.04}$ (26)

Correlation	Reversal	Eu–Na[13]	Eu–Na[14]	Eu–Na[15]	Eu–Na[16]	Eu–Na[17]	In–Sm[18]
Point	Age (Ma)	41.2°N, 29.4°W	51.6°N, 30.0°W	53.8°N, 35.2°W	60.1°N, 29.3°W	68.7°N, 17.3°W	7.7°N, 59.4°E
C1n(o)	0.781	$18.63^{+0.64}_{-0.54}$ (14)	$19.89^{+0.51}_{-0.50}$ (44)	$21.35^{+0.40}_{-0.39}$ (71)	$20.82^{+0.19}_{-0.18}$ (354)	$15.12^{+0.41}_{-0.33}$ (64)	$20.49^{+0.46}_{-0.46}$ (74)
C2n(y)	1.778	—	$42.59^{+0.35}_{-0.46}$ (40)	$40.72^{+0.40}_{-0.30}$ (72)	$39.42^{+0.18}_{-0.10}$ (334)	$31.63^{+0.33}_{-0.41}$ (60)	$42.59^{+0.35}_{-0.46}$ (57)
C2n(c)	1.8615	$43.39^{+0.75}_{-0.65}$ (14)	—	—	—	—	—
C2An.1(y)	2.581	$58.89^{+0.65}_{-0.75}$ (15)	$57.75^{+0.41}_{-0.40}$ (44)	$57.30^{+0.40}_{-0.29}$ (71)	$55.03^{+0.19}_{-0.18}$ (354)	$44.87^{+0.41}_{-0.32}$ (71)	$62.11^{+0.51}_{-0.46}$ (68)
C2An.3(o)	3.596	$80.75^{+0.54}_{-0.54}$ (16)	$78.76^{+0.40}_{-0.51}$ (44)	$79.15^{+0.30}_{-0.39}$ (71)	$74.56^{+0.27}_{-0.28}$ (221)	$63.02^{+0.33}_{-0.41}$ (62)	$81.68^{+0.46}_{-0.46}$ (52)
C3n.1(y)	4.187	$94.21^{+0.64}_{-0.75}$ (15)	$90.77^{+0.61}_{-0.60}$ (37)	$88.89^{+0.49}_{-0.50}$ (56)	$86.08^{+0.37}_{-0.28}$ (216)	$73.89^{+0.57}_{-0.65}$ (34)	—

Correlation	Reversal	In–Sm[19]	In–Sm[20]	In–Sm[21]	In–Sm[22]	Nb–Na[23]	Nb–Na[24]
Point	Age (Ma)	6.1°N, 60.9°E	4.6°N, 62.6°E	2.9°N, 65.6°E	1.8°S, 67.8°E	25.1°N, 44.7°W	35.6°N, 45.0°W
C1n(o)	0.781	$21.96^{+0.49}_{-0.49}$ (71)	$22.57^{+0.51}_{-0.52}$ (60)	$25.65^{+0.42}_{-0.49}$ (83)	$26.37^{+0.53}_{-0.46}$ (60)	$21.09^{+0.7}_{-0.8}$ (33)	$16.72^{+0.35}_{-0.35}$ (54)
C1r.1n(c)	1.03	—	—	—	—	$27.88^{+0.90}_{-1.0}$ (22)	$21.89^{+0.44}_{-0.35}$(45)
C2n(y)	1.778	$45.81^{+0.42}_{-0.31}$ (67)	$48.81^{+0.32}_{-0.39}$ (76)	$52.76^{+0.35}_{-0.35}$ (68)	$57.01^{+0.38}_{-0.46}$ (52)	—	—
C2n(c)	1.8615	—	—	—	—	$44.87^{+0.60}_{-0.70}$ (39)	$37.12^{+0.44}_{-0.35}$ (46)
C2An.1(y)	2.581	$65.40^{+0.48}_{-0.43}$ (81)	$70.60^{+0.39}_{-0.39}$ (94)	$74.30^{+0.48}_{-0.42}$ (74)	$83.30^{+0.53}_{-0.46}$ (69)	$60.26^{+0.61}_{-0.61}$ (55)	$54.02^{+0.50}_{-0.51}$ (32)
C2An.3(o)	3.596	$88.21^{+0.48}_{-0.49}$ (52)	$94.39^{+0.45}_{-0.45}$ (63)	$102.45^{+0.42}_{-0.34}$ (85)	$113.78^{+0.46}_{-0.53}$ (53)	$84.25^{+0.7}_{-0.7}$ (32)	$75.56^{+0.61}_{-0.61}$ (21)

zero-seafloor-age intercepts (Fig. 5a). We determined the probability that random errors in the estimated opening distances could be responsible for such a positively-biased distribution of distance-axis intercepts through a simple statistical test. We first inverted each of the 81 age-distance sequences imposing the requirement that their best-fitting slopes pass through the origin, corresponding to zero outward displacement. This model yields a cumulative weighted least-squares misfit χ^2 of 2414. We then simultaneously inverted all 81 age-distance sequences to estimate their individual best-fitting opening rates along with a single, globally uniform distance-axis intercept (e.g. tantamount to requiring that outward displacement be the same in all 81 study areas). This model yields a best-fitting intercept value of 2.5 $\pm$ 0.1 km and $\chi^2 = 1356$, $\sim$45 per cent smaller than the previous model. The probability that the improved fit is a random outcome of fitting the data with one additional parameter is vanishingly small, only one part in 10^{39}.

Table 2. (*Continued.*)

Correlation	Reversal	Nb–Na[25]	Nb–Sa[26]	Nb–Sa[27]	Nb–Sa[28]	Nb–Sa[29]	
Point	Age (Ma)	37.8°N, 31.5°W	26.2°S, 13.7°W	33.1°S, 14.4°W	51.7°S, 5.6°W	54.4°S, 1.2°W	
C1n(o)	0.781	$16.65^{+0.93}_{-0.92}$ (9)	$26.65^{+0.44}_{-0.34}$ (45)	$25.42^{+0.33}_{-0.45}$ (67)	$23.73^{+0.61}_{-0.61}$ (14)	$23.58^{+0.70}_{-0.69}$ (18)	—
C1r.1n(c)	1.03	$22.12^{+1.01}_{-0.93}$ (9)	$35.64^{+0.44}_{-0.33}$ (38)	$35.74^{+0.33}_{-0.45}$ (56)	$31.91^{+0.62}_{-0.71}$ (13)	$30.65^{+0.59}_{-0.60}$ (21)	—
C2n(c)	1.8615	$35.49^{+0.50}_{-0.51}$ (24)	$61.95^{+0.34}_{-0.44}$ (40)	$61.93^{+0.44}_{-0.33}$ (76)	$56.56^{+0.51}_{-0.51}$ (20)	$54.63^{+0.49}_{-0.60}$ (24)	—
C2An.1(y)	2.581	$50.29^{+0.50}_{-0.51}$ (25)	$85.49^{+0.55}_{-0.56}$ (20)	$85.68^{+0.33}_{-0.44}$ (52)	$78.66^{+0.81}_{-0.72}$ (15)	$76.12^{+0.80}_{-0.70}$ (16)	—
C2An.2(c)	3.1615	$104.59^{+0.55}_{-0.55}$ (18)	—	—	—	$86.37^{+1.1}_{-1.1}$ (14)	—
C2An.3(o)	3.596	$68.45^{+0.84}_{-0.86}$ (13)	$118.46^{+0.45}_{-0.55}$ (19)	$117.31^{+0.33}_{-0.33}$ (56)	—	—	—

Left column specifies magnetic anomalies correlated for the analysis. Anomaly names are from Cande & Kent (1992). '(o)', '(y)', and '(c)' refer respectively to old and young reversal edges, and centre of the specified anomaly. Reversal ages are from Lourens *et al.* (2004). Reconstructed opening distances and their standard errors are in kilometres along a flow line, passing through the location in the column header. Parenthetical numerals following opening distances are the number of anomaly crossings that are used to constrain a given distance. Plate abbreviations: An, Antarctic; Au, Australia; Cp, Capricorn ; Eu, Eurasia; In, India; NA, North America; Nb, Nubia; Pa, Pacific; SA, South America and Sm, Somalia. Coordinates specify the location where the opening distances are calculated. (1) Pacific–Antarctic rise axial valley segments, 175°W–150°W; (2) Pacific–Antarctic rise axial rise segments, 55°S–49°S; (3) Pacific–Antarctic rise axial rise segments, 45°S–37°S; (4) Southeast Indian Ridge (SEIR) axial rise segments, 79°E–102°E; (5) SEIR shallow axial valley segments, 103°E–120°E; (6) SEIR axial valley segments, 121°E–127.4°E; (7) SEIR axial rise segments, 127.4°E–138°E; (8) Central Indian Ridge (CIR) at 10°S; (9) CIR, 12°S–17°S; (10) CIR, 18°S–20°S; (11) CIR, 20°S–23°S; (12) CIR, 23.5°S–25.5°S; (13) Mid-Atlantic Ridge (MAR) north of Azores triple junction, 40.5°N–42°N; (14) MAR south of C. Gibbs fracture zone, 51°N–52°N; (15) MAR north of Gibbs fracture zone, 53°N–54.5°N; (16) Reykjanes Ridge, 57°N–63°N; (17) Kolbeinsey Ridge, 67.3°N–70°N; (18) Carlsberg ridge (CR), 58°E–60°E; (19) CR, 60°E–61.6°E; (20) CR, 61.6°E–64.2°E; (21) CR, 64.2°E–66.7°E; (22) CR, 0°S–4°S; (23) MAR, 21.5°N–28°N; (24) MAR, 34.5°N–37°N; (25) MAR, 37°N–38°N; (26) MAR, 25°S–27°S; (27) MAR, 31°S–34.5°S; (28) MAR, 50.5°S–52.2°S; (29) MAR, 54°S–54.8°S.

We next inverted each of the 81 age-distance sequences to estimate a best-fitting slope and intercept for each. The intercept values for this more complex model range from 2 to 8 km for slow spreading rates and 1 to 4 km for faster rates (Fig. 5a), and the cumulative least-squares misfit is $\chi^2 = 525$. The improvement in the fit is significant at a level of one part in 10^{17} relative to the fit of the previous model in which we estimated a single zero-age intercept for all 81 age-distance sequences. Consequently, the variation in the values of the zero-age intercepts is highly significant.

Reduced χ^2 (e.g. the weighted least-squares misfit normalized by the degrees of freedom) is 2.4 for the model in which separate slopes and intercepts are estimated for each of the 81 age-distance sequences, higher than the value of 1.0 that is expected if spreading rates have remained constant over the time sampled by each age-distance sequence and if the opening distance uncertainties are approximately correct. The average misfit to the observed opening distances is several hundred metres greater than their assigned uncertainties. Possible reasons for these modestly larger misfits are examined in Section 3.2.4

The 81 age-distance sequences are thus fit significantly better by a model in which magnetic reversals are shifted outward from the axis of seafloor spreading with respect to their idealized locations. The average intercept value of 2.5 ± 0.1 km represents the total outward displacement between two, same-age reversal boundaries that flank a spreading segment. By implication, individual reversal boundaries are shifted by an average of 1.25 ± 0.07 km outward from their idealized locations.

3.2 Results from 29 grouped age-distance sequences

3.2.1 Linear regressions

Based on the obvious similarity of the magnitudes of outward displacement within many of the 81 regions into which we initially subdivided the data, we next determined best-fitting slopes and intercepts for the 29 age-distance sequences that we derived from the geographically consolidated subsets of the anomaly crossings (Table 2). The resulting 29 zero-age intercepts are uniformly positive (Fig. 5b) and exhibit scatter that is a factor-of-two smaller than for the 81 age-distance sequences. Their mean value of 2.8 ± 0.3 km is insignificantly larger than that for the 81 age-distance sequences (2.5 km) and the cumulative normalized least-squares misfit to the 29 age-distance sequences is only 4 per cent higher than that for the 81 age-distance sequences, even though many fewer adjustable parameters (58 versus 162) are used to fit the 29 age-distance sequences. The more consistent intercept values and comparable fits of the two models validate our decision to fit the data with fewer adjustable parameters.

When plotted along their respective plate boundaries (Figs 6a–f), the 29 values for outward displacement show several interesting patterns. Outward displacement along the northern Mid-Atlantic Ridge (Fig. 6d) exhibits the largest variation of any spreading centre, with values of 1–2 km near the Azores triple junction and along the Kolbeinsey Ridge north of Iceland, but much larger values of 5–6 km at intermediate locations along the Reykjanes Ridge, south of Iceland and north of the Charlie Gibbs fracture zone (52.5°N). Along the Southeast Indian Ridge (Fig. 6b), outward displacement changes abruptly at the eastern edge of the Australia–Antarctic discordance, from 3 ± 1 km within the discordance to less than 1 km immediately east of the Discordance. We next employ methods described in Section 2.3 to determine whether these apparent variations are robust.

3.2.2 Effect of the rigid plate constraint

Figs 6(a)–(f) and 7 show the best-fitting estimates of outward displacement for the 29 study regions described above, when we invert simultaneously all the anomaly crossings from a plate boundary

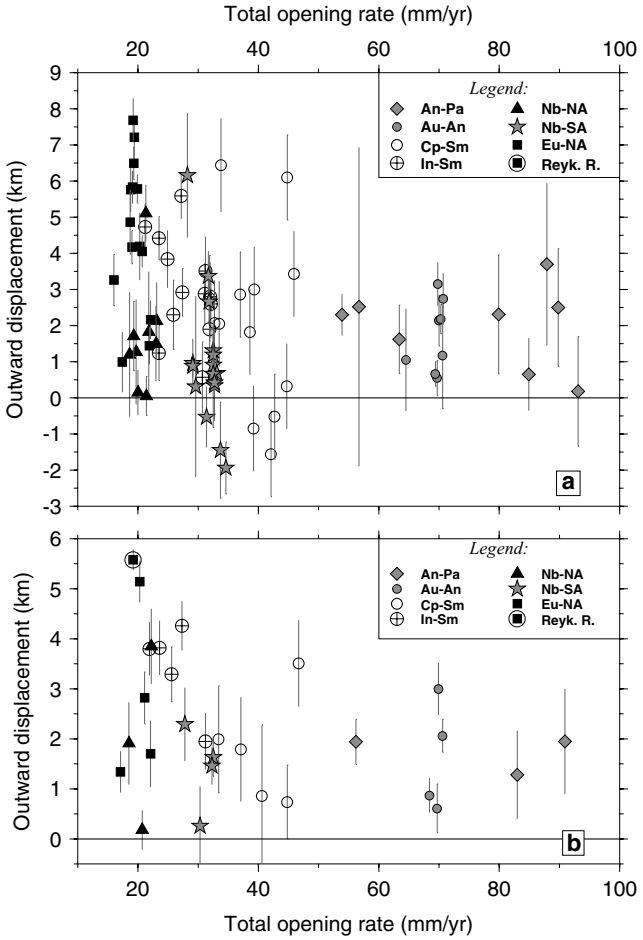

Figure 5. Kinematic estimates of outward displacement as a function of spreading rate, dividing the data into 81 local age-distance sequences (a) or 29 more clustered sequences (b). Estimates are derived from the linear regression of the time-series of opening distances, derived from optimized reconstructions of anomaly crossings for single spreading segments or for geographically clustered spreading segments with similar axial morphology. Standard errors are shown.

to enforce the rigid plate assumption (Section 2.3). The weighted average value of outward displacement for these 29 study regions is 2.2 ± 0.3 km (Fig. 7), consistent with the results reported above. However, the variance of the 29 estimates relative to this mean value is 30 per cent smaller than is the variance of the estimates that do not satisfy the rigid plate constraint (Section 3.2.1). The improvement in the consistency of the results indirectly indicates that the revised estimates are more accurate. In particular, the revised estimates along the Nubia–North America plate boundary (Fig. 6d), the sparsely surveyed southern end of the Nubia–South America plate boundary (Fig. 6e) and the Capricorn–Somalia plate boundary (Fig. 6f), each show less scatter than do the estimates that were derived without applying a rigid plate constraints. These support our earlier assertion that the propagation of information about the rate of angular opening from densely surveyed areas of the plate boundary to more sparsely surveyed areas via enforcement of a rigid plate assumption can improve estimates of outward displacement along sparsely surveyed parts of a plate boundary.

The revised estimates confirm that outward displacement along slow spreading centres varies in magnitude by roughly a factor of two more than along faster spreading centres, where all of our estimates are smaller than 3 km (Fig. 7). For the Eurasia–North America and Australia–Antarctic plate pairs, our estimates of outward displacement exhibit similar variations with location whether or not we enforce plate rigidity (Figs 6b and d), suggesting that the estimates are robust and the variations are hence real.

3.2.3 *Effect of reversal age uncertainties*

All of the results described above are derived assuming that magnetic reversal ages are perfectly known, which is clearly untrue. We therefore evaluated the influence of likely errors in the estimated reversal ages on our estimates of outward displacement by assigning realistic uncertainties to those ages and repeating the linear regressions of all 29 age-distance sequences. Lourens *et al.* (2004) estimate that uncertainties in the astronomically-tuned ages of young reversals are ±0.1–0.2 per cent, which implies that the absolute age uncertainties for the anomalies employed in our analysis are ±1000 to ±5000 yr.

To evaluate the sensitivity of our results to such errors, we assigned more conservative errors of ±0.005 Myr (±5000 yr) to the estimated ages for C1n(o) and C1r.1 and ±0.01 Myr (±10 000 yr) to the older reversals and repeated our linear regressions of the 29 age-distance sequences and their reversal age and opening distance uncertainties. The resulting values for outward displacement range from 0.2 km to 5.7 km and differ on average by only 0.11 km from the estimates we derived by assuming that reversal ages are perfectly known. Our estimates of outward displacement are thus robust with respect to possible errors in the reversal ages we use. By implication, future revisions to magnetic reversal age estimates should not significantly alter our estimates of outward displacement, provided that such revisions are smaller than the presumably conservative age uncertainties that we employ above.

3.2.4 *Consistency with assumption of constant spreading rates*

The misfits of the 29 best-fitting, rigid-plate models to their corresponding opening distances (Fig. 8) are typically smaller than 1 km for the Capricorn–Somalia, Eurasia–North America and Nubia–Somalia age-distance sequences (Fig. 8) and are otherwise typically smaller than 2 km, close to the estimated uncertainties.

If seafloor spreading rates have remained constant during the intervals spanned by our data and we have correctly estimated the uncertainties in the opening distances, then the normalized misfits to the 29 age-distance sequences should exceed the 95 per cent misfit threshold for only 5 per cent (1–2) of the age-distance sequences. Using reduced chi-square as our measure of misfit, we instead find that the misfits exceed their expected 95 per cent misfit threshold for 7 of the 29 age-distance sequences. The higher-than-expected misfits could be explained several ways, including opening distance uncertainties that might be too small, possible changes in motion for one or more of the seven plate pairs that are included in our analysis or possible changes in the magnitude of outward displacement as a function of seafloor age. We briefly examine each of these possibilities below.

Two of the seven age-distance sequences that are misfit at a higher than expected level are from the India–Somalia plate boundary, raising the question of whether India–Somalia motion may have changed significantly over the past few million years. Using numerous data from this densely mapped boundary, Merkouriev & DeMets (2006), however, conclude that motion since ∼8 Ma has changed by no more than ±2 per cent, equivalent to a maximum change

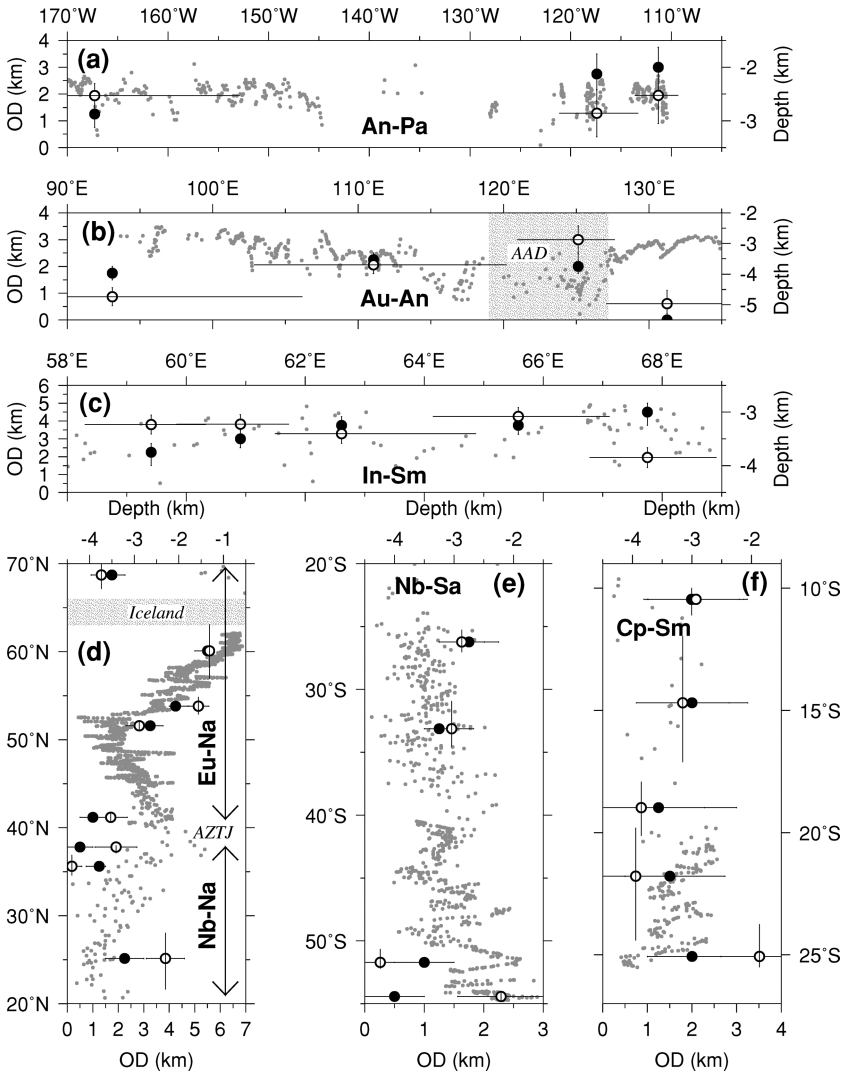

Figure 6. Estimates of outward displacement at 29 locations along the mid-ocean ridge system from magnetic reversals that flank spreading segments centred on these locations. Filled and open circles are derived with and without rigid plate constraints, respectively, as described in the text. Grey dots show axial depths. Horizontal lines in (a)–(c) and vertical lines in (d)–(f) indicate the geographic limits of the anomaly crossings that were used for individual estimates of outward displacement. Abbreviations: AAD, Australia–Antarctic Discordance; AZTJ, Azores triple junction; An-Pa, Antarctic–Pacific; Au-An, Australia-Antarctic; In-Sm, India–Somalia; Eu-Na, Eurasia–North America; Nb-Na, Nubia–North America; Nb-Sa, Nubia–South America and Cp-Sm, Capricorn–Somalia.

in the seafloor spreading rate of only ± 0.6 mm yr^{-1}. Similarly, a third age-distance sequence with a higher-than-expected misfit is from the densely surveyed Eurasia–North America plate boundary, where Merkouriev & DeMets (2008) conclude that motion since 6.7 Ma has remained constant within a limit of ± 2 per cent, equivalent to a maximum change in spreading rate of only ± 0.5 mm yr^{-1}. The evidence for constant motion for both of these two plate pairs after correcting their respective motions for constant-valued outward displacement argues against a change in motion or age-dependent outward displacement as possible explanations for their higher than expected misfits. Consequently, the misfits seem more likely to be a result of underestimated uncertainties in our reconstructed opening distances.

The remaining four age-distance sequences with higher-than-expected misfits are each from a different plate boundary. If the higher-than-expected misfits for any one of these four plate pairs were caused by a change in motion over the past several Myr, most or all of the other age-distance sequences for that plate pair should also be poorly fit by their corresponding constant-motion model. Given that this is not the case, a change in motion seems unlikely for any of the four.

The most likely explanation for the higher-than-expected misfits is that the formal uncertainties for our opening distances, which are propagated rigorously from assumed random errors in the anomaly crossing locations, are too small. For example, if we propagate an additional systematic uncertainty of only ± 0.3 km into the formal opening distance uncertainties, the misfits to all but one of the 29 age-distance sequences are reduced below the 95 per cent significance threshold. An additional systematic error of 0.3 km is well within the $\sim$1 km range of likely systematic bias that Merkouriev & DeMets (2006, 2008) report from reconstructions of magnetic reversals along the densely surveyed Eurasia–North America and India–Somalia plate boundaries. Biases of several hundred metres in magnetic reversal locations might be caused by several factors, including unmodelled seafloor topography, systematic errors in pre-GPS shipboard or airplane navigation or modest

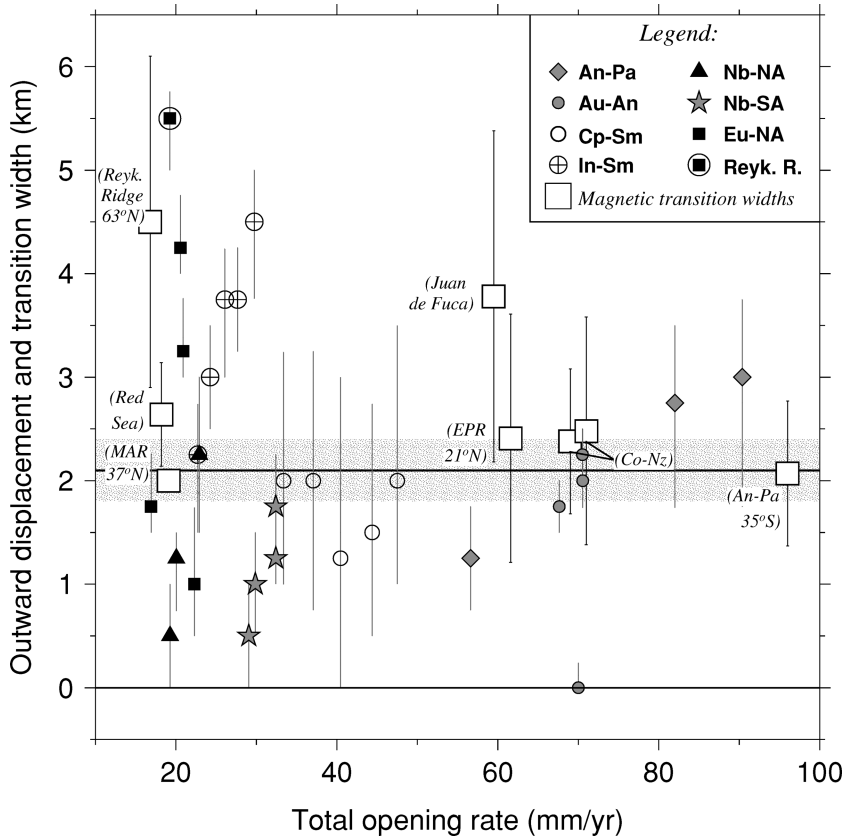

Figure 7. Comparison of magnetic polarity transition zone widths determined from near-bottom marine magnetic profiles (open squares) (Sempere *et al.* 1987, 1990) and kinematic estimates of outward displacement determined via simultaneous inversion of all data from a given plate boundary and subject to the constraint of plate rigidity. The total outward displacement between same-age magnetic reversals that flank a seafloor spreading centre is approximately equal to the width of the polarity transition zone (see text). Heavy line and shaded area show mean value of the kinematic estimates and its standard error, respectively. Abbreviations: Co-Nz, Cocos–Nazca; EPR, East Pacific Rise; MAR, Mid-Atlantic Ridge. Standard errors are shown.

variations in the widths of polarity transition zones along spreading centres.

3.3 Relationships of axial morphology and depth to variations in outward displacement

Fig. 9 shows 0.781 Ma opening distances derived from ∼300 crossings of the old edge of Anomaly 1 for 28 spreading segments between 78°E and 138°E along the Southeast Indian Ridge. Significant departures from the expected sinusoidal change in the width of Anomaly 1 are observed and are clearly correlated with changes in axial morphology and depth. The most striking change occurs at the eastern edge of the Australia–Antarctic discordance (127.5°E), where Anomaly 1 for spreading segments located within the discordance is ∼3 km wider than for spreading segments immediately east of the discordance. This change coincides with an abrupt change in both axial morphology and depth for spreading segments within and east of the discordance.

A similar correlation occurs from 103°E to 120°E, west of the discordance, where detailed multibeam surveys of the ridge define a more gradual transition in axial morphology (Cochran *et al.* 1997). In this region, Anomaly 1 for ridge segments that are characterized by shallow axial valleys is 1–1.5 km wider than extrapolated from both a GPS estimate of Australia–Antarctica motion and from the widths of Anomaly 1 across axial rise segments west of 103°E and east of 127.5°E. The observations thus indicate that outward displacement is the widest for ridge segments with deep axial valleys, is intermediate in magnitude for shallow axial valley segments and is the smallest for axial rise segments.

Based on these results, we searched along other spreading centres for evidence of a correlation between outward displacement and either axial morphology or seafloor depth. Seafloor depths in the study areas along the other six plate boundaries that are included in our analysis, however, show no correlation with the magnitude of outward displacement (Fig. 10). Values for outward displacement span their entire observed range whether for spreading segments whose depths fall within the most common range (2.5–3.1 km) or for spreading segments whose depths are shallower due to the influence of one or more nearby hotspots. Moreover, outward displacement decreases in magnitude with increasing seafloor depth along the Reykjanes and Mid-Atlantic ridges south of Iceland (Fig. 6d), opposite the pattern exhibited along the Southeast Indian Ridge, where shallower depths are correlated with smaller-magnitude outward displacement (Fig. 6b).

Elsewhere, we find no correlation between the magnitude of outward displacement and axial morphology. For example, outward displacement along the Capricorn–Somalia and Nubia–South America plate boundaries, where axial valley morphologies predominate, has the same magnitude as along the Pacific–Antarctic rise, where axial rise morphologies predominate in the areas sampled in our study. In the north Atlantic, a monotonic southward decrease in outward displacement between Iceland and the Azores hotspot (Fig. 6d)

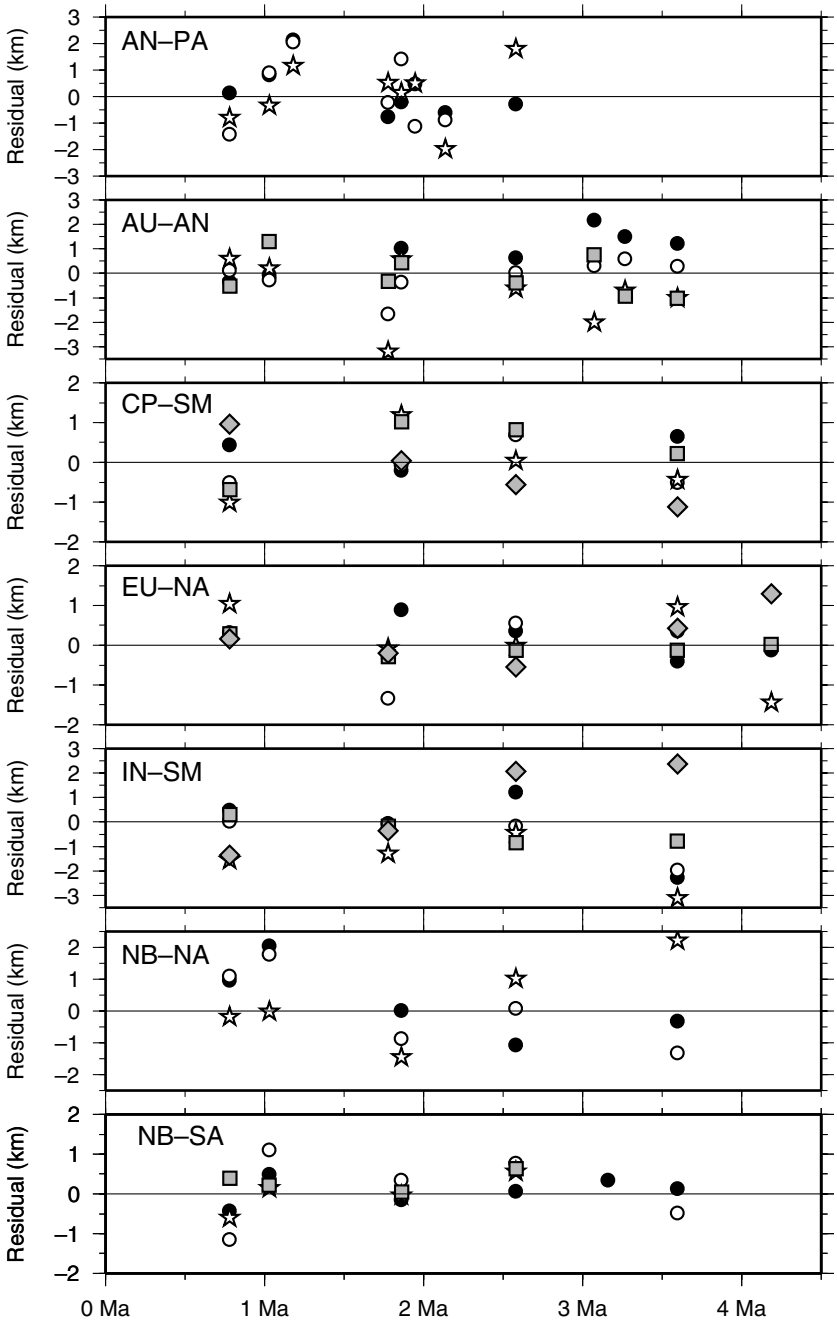

Figure 8. Fits to 29 age-distance series in Table 2 reduced by opening distances predicted from models that simultaneously estimate the best constant angular opening rate for a plate boundary and best values of outward displacement for each study area along the boundary (Section 3.2.2). Error bars are omitted for clarity. Different symbols specify the opening distances for different study areas along a boundary. Plate abbreviations are given in caption to Fig. 2. Not shown are two outliers that contribute little to the solutions due to their large uncertainties, one for NB–SA (−6.0 km at 3.16 Ma) and the other for AN–PA (7.6 km at 2.58 Ma).

coincides with a change from axial rise morphologies along the Reykjanes Ridge just south of Iceland to axial valley morphology between the Charlie Gibbs fracture zone and Azores triple junction. This pattern is opposite that observed along the Southeast Indian Ridge (Fig. 9c).

In absence of any evidence for a globally-consistent correlation between outward displacement and spreading centre depth or morphology, we conclude that other factors must determine its magnitude. In Section 4.2, we demonstrate that forward modelling of synthetic magnetic profiles that use a plausible range of assumed magnetic layer thicknesses, intensities and layer geometries yields outward displacement comparable in magnitude to our kinematic estimates.

4 DISCUSSION

4.1 Comparison to magnetic polarity transition widths

To first order, the crossover from positively to reversely magnetized crust within a magnetic reversal transition zone should coincide with

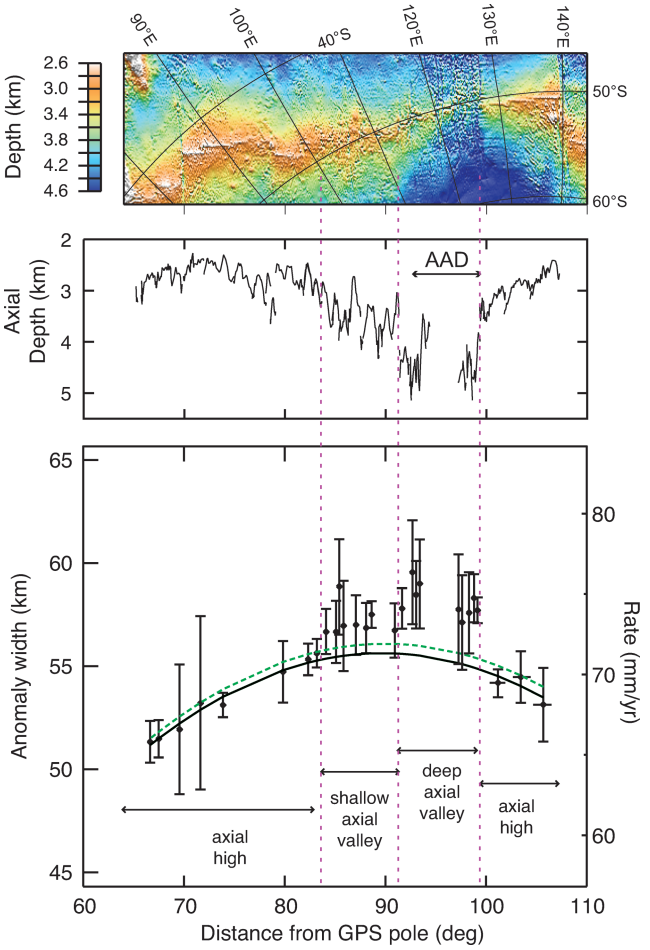

Figure 9. (a) Seafloor depth map for Southeast Indian Ridge, 78°E–140°E. Depths are from Sandwell & Smith (1997). (b) Depth to Southeast Indian Ridge spreading axis. (c) Width and full spreading rate for Anomaly 1 as a function of spreading axis morphology along the Southeast Indian ridge with spreading axis moropogy annotated. Circles show anomaly width for individual spreading segments estimated from reconstructions of ∼300 digitized anomaly crossings. Error bars are 95 per cent confidence limits. Solid line shows anomaly width predicted by a finite rotation that best reconstructs anomaly crossings from only the axial rise segments (14.0°N, 38.7°E, 0.501° Myr^{-1}). Dashed curve shows rate predicted by the Australia–Antarctica GPS angular velocity vector (13.9°N, 39.1°E, 0.647° Myr^{-1}). Horizontal axis for all three panels shows angular distance from the latter pole.

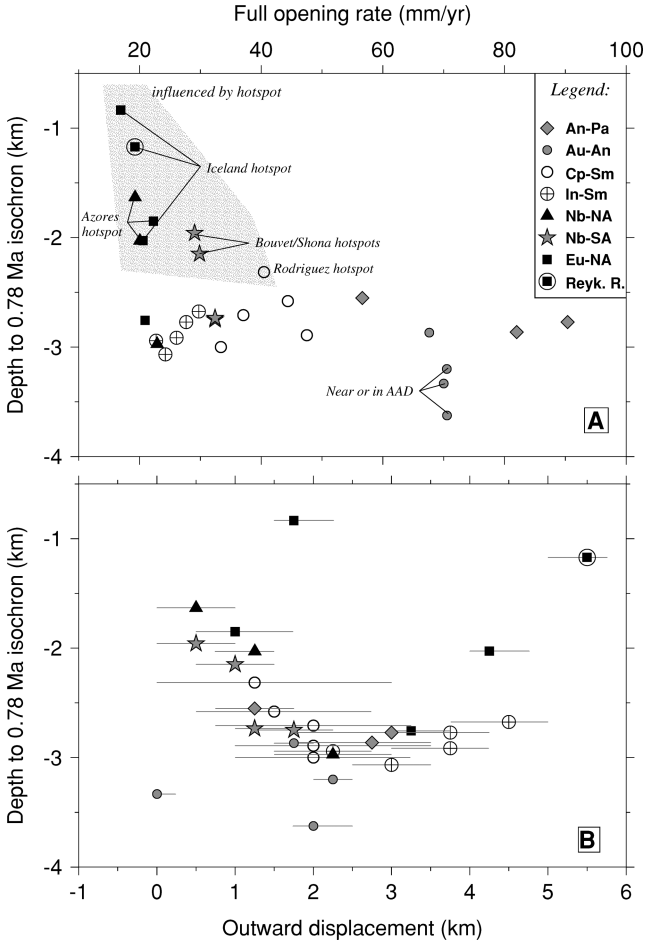

Figure 10. (a) Anomaly-1-age seafloor depth versus full opening rate for the 29 study areas discussed in the text. AAD, Australia–Antarctic Discordance. Shaded area encloses estimates for which depths are influenced by nearby hotspots. (b) Outward displacement estimates and Anomaly-1-age seafloor depth in each study area. Values for outward displacement are from Fig. 7. Horizontal lines show estimated standard errors.

the midpoint of the transition zone (Macdonald *et al.* 1983). The summed outward shift of two same-age magnetic polarity transitions across a spreading segment should therefore approximately equal the full width of a polarity transition zone. Consequently, direct estimates of magnetic polarity transition zone widths from inversions of near-bottom seafloor magnetic profiles provide an independent determination of outward displacement that can be compared to our kinematic estimates.

Fig. 7 shows full transition zone widths estimated by Sempere *et al.* (1987, 1990), from deeply towed magnetic profiles of young oceanic crust, for a wide range of seafloor spreading rates. The polarity transition widths are typically 2–3 km and thus agree remarkably well with many of our kinematic estimates. Macdonald (1977) further report transition zone widths of 1–8 km from near-bottom magnetic profiles of the Mid-Atlantic Ridge near 37°N, with most widths between 1 and 2 km. These agree with our own kinematic estimates from the Nubia–North America plate boundary (Fig. 6d), which range from 0.5 to 2.2 km. Along the Reykjanes Ridge, where we find evidence for anomalously wide outward displacement of 5.5 ± 0.4 km (Figs 6d and 7), Sempere *et al.* (1990) determine a polarity transition zone width of 4.5 ± 1.6 km from inversions of shallow-water magnetic profiles from the Reykjanes Ridge just south of Iceland. The good agreement between these independent estimates confirms the existence of anomalously wide outward displacement along the Reykjanes Ridge, the kinematic implications of which are described by Merkouriev & DeMets (2008).

4.2 Effects of magnetic source geometries: forward modelling

In areas where the primary source of magnetic anomalies is in the upper section of the oceanic crust and the source-layer thickness is significantly less than the water depth, as is typically the case along most of the mid-ocean ridge system, outward displacement should be about the same as the width of the magnetic reversal transition zone. We therefore test whether observed variations in the width of outward displacement along a plate boundary are attributable to plausible along-axis variations in the character of the magnetic

source layer. Previous studies systematically describe the influence of the assumed source layer geometry, its magnetic intensity distribution and seafloor spreading rate on the character of marine magnetic anomalies (e.g. Blakely 1976; Cande & Kent 1976; Blakely & Lynn 1977; Kidd 1977; Schouten & Denham 1979; Arkani-Hamed 1989; Dyment & Arkani-Hamed 1995; Dyment *et al.* 1997). These studies lay the conceptual groundwork for the simple forward modelling that we undertake below in which we generate synthetic magnetic profiles from alternative polygonal models of the source layer to examine their effect on outward displacement.

Following Kidd (1977), we assume that the magnetic source consists of dykes with vertical polarity boundaries that form exactly at the axis (Fig. 1), an overlying flow layer with inward-dipping polarity boundaries that result from the range of distances over which flows accumulate from the axis and an underlying gabbro layer with outward-dipping polarity boundaries that are caused by cooling through the magnetic blocking temperature (∼500 °C) at a significant distance from the spreading axis. Our models do not incorporate any subsidence, faulting or tilting of pre-existing flows that are buried off-axis by newer flows nor do they include any decrease in the intensity of magnetization with age. Moreover, because we are trying to fit the magnetic structure at polarity boundaries, but not close to the axis of spreading, we use seafloor magnetization values that are lower than have been measured on zero-age basalts.

We first demonstrate that plausible variations in the nature of the source layer can be used to explain the unusually abrupt change in the width of the Anomaly 1n at the eastern edge of the Australia–Antarctic discordance (labelled 'AAD' in Fig. 9), where our kinematic analysis indicates that outward displacement changes from 3–4 km within the AAD (124°–127°E in Fig. 6b) to 1 km east of the AAD (128°–136°E). The observations that are pertinent to the magnetic source layer that we constructed to model magnetic anomalies in this region are as follows:

(1) Magnetic anomaly amplitudes change abruptly at the eastern edge of the discordance (Anderson *et al.* 1980), with higher-amplitude anomalies that are found east of the AAD associated with higher-iron lavas. This abrupt change is well illustrated by the factor-of-two difference in the anomaly amplitudes for the *Eltanin* 39 profile, which crosses the ridge near 134°E (Fig. 11a), ∼450 km east of the AAD and the *Boomerang* 05 profile, which crosses the ridge at 127.35°E (Fig. 11b), within the AAD. Both

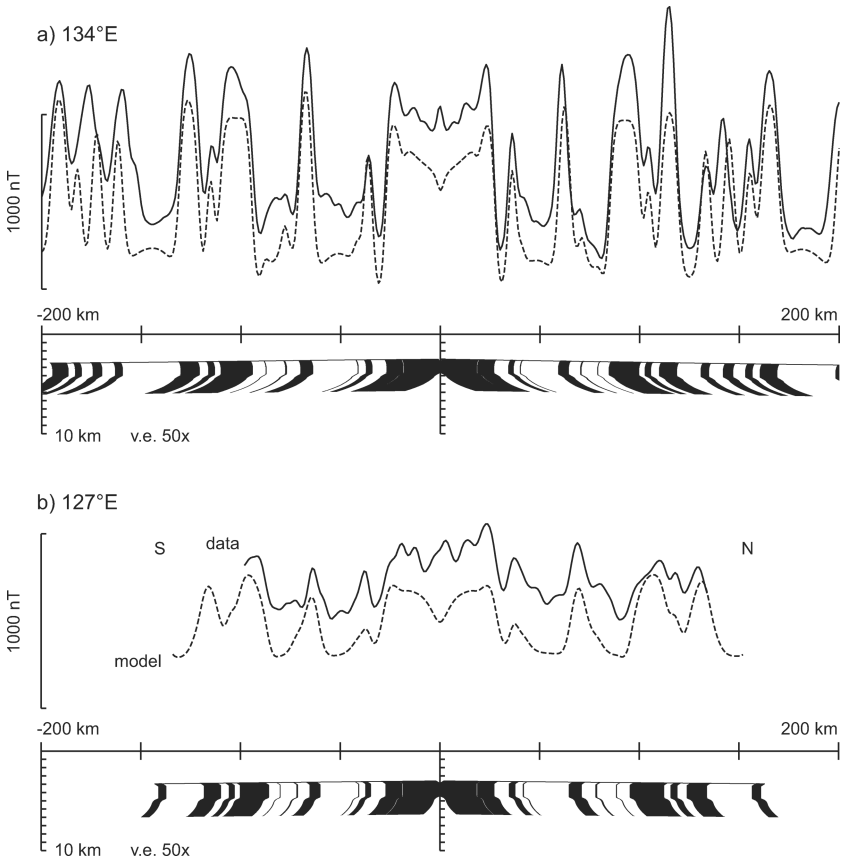

Figure 11. Observed (deskewed) and synthetic magnetic anomalies from the Southeast Indian Ridge for an axial-high region east of Australia–Antarctic discordance (AAD) at 134°E (a) and an axial-valley region just within AAD at 127°E (b). Models are calculated from a source layer with inward-dipping polarity boundaries in the top flow layer, vertical boundaries formed at the axis in the middle dyke layer, and outward-dipping boundaries in the lower gabbro layer. The model for 134°E (a) is dominated by flows and dykes forming within 1 km of the axis, with magnetization of 7 A m^{-1} and thickness of 0.7 km for the flow layer, 3 A m^{-1} and 0.9 km for the dyke layer and 1 A m^{-1} and 2.2 km for the gabbro layer, yielding an outward displacement of ∼1 km. For 127°E, upper layers do not dominate the model, with magnetization of 1.8 A m^{-1} and thickness of 0.5 km for flows, 1.5 A m^{-1} and 1.2 km for dykes, and 1.5 A m^{-1} and 2.2 km for gabbro, yielding outward displacement of ∼4 km. Full spreading rates are regional Chron 1n to Chron 3 Australia–Antarctic averages of 69.3 mm yr^{-1} at 134°E and 70.2 mm yr^{-1} at 127°E, with moderate asymmetry adjusted to fit the observed profiles. NGDC cruise IDs for data profiles are ELT39 (a) and BMRG05MV (b). No effort has been made to model the magnetic high at the centre of Anomaly 1, thereby accounting for the poor fit to this feature.

profiles closely follow Australia–Antarctic flow lines and are typical of other profiles from this region.

(2) Seafloor within the AAD is anomalously deep and has unusually rough bathymetry for its spreading rate (Weissel & Hayes 1974).

(3) Seismic refraction data show that the part of the AAD that is characterized by deep seafloor, rough topography and low-magnitude magnetic anomalies also has anomalously thin crust (Tolstoy *et al.* 1995; Kojima *et al.* 2003).

The magnetic source model that we employ to model the *Eltanin* 39 profile east of and outside the AAD consists of strongly magnetized flows and upper-crustal dykes that form and magnetize within 1 km of the axis (Fig. 11a) and more deeply seated, weakly magnetized dykes and gabbros that are assumed to acquire a time-delayed magnetization, away from the axis due to slow cooling (Blakely 1976; Cande & Kent 1976; Kidd 1977). The synthetic magnetic profile based on this source model and the observed constant seafloor spreading rate fits the *Eltanin* 39 magnetic profile well, with the good fit driven primarily by sharp transitions in the strongly magnetized shallower layers, but with the longer-wavelength components of the profile well fit by the more weakly magnetized deep layer.

Our magnetic source model for seafloor, located within the Australia–Antarctic discordance, assumes that dykes, gabbros and possibly serpentinized peridotites that cool slowly at deeper levels in the crust and possibly uppermost mantle and hence acquire their magnetization several kilometres away from the axis of seafloor spreading, contribute more to the surface magnetic anomalies than does a strongly magnetized upper crustal layer. General considerations suggest the plausibility of such a model. The rough, often chaotic seafloor fabric, presence of megamullion structures, high inferred basement densities and common recovery of gabbros and serpentinites dredged within the discordance (Christie *et al.* 1998; Okino *et al.* 2004) all suggest that the flow layer in the AAD is generally thin, locally absent and seldom extends several kilometres from its source. Differences in magma chamber processes lead to lower Fe flows (and presumably dykes) within the AAD, leading to lower magnetization, given the well documented strong correlation between Fe content and magnetization intensity (Vogt & Johnson 1973; Anderson *et al.* 1980; Gee & Kent 1998). Because less Fe is fractionated into flows and dykes in the AAD, gabbros should have higher Fe content and possibly higher magnetization. Finally, the anomalously rough seafloor implies that faulting also plays an important role in extension within the AAD, possibly allowing greater hydrothermal circulation and hence more rapid cooling at depth. If so, this implies that the Curie isotherm may be steeper, thereby leading to a larger-amplitude contribution from the slowly cooled, deeper layers than would otherwise be the case.

A synthetic magnetic profile that uses the above source model (Fig. 11b) nicely matches the *Boomerang* 05 profile at 127°E, provided that the more deeply seated dykes and gabbros acquire their magnetization 1–4 km from the spreading axis (also see Dyment *et al.* 1997). Relative to an idealized source model, in which reversal boundaries are assumed to be vertical and magnetization intensity is assumed to be uniform, the magnetic source model described above predicts that polarity transitions are shifted outwards by several kilometres, consistent with the available observations.

Further support for our assumption of a deeper dyke- and gabbro-dominated magnetic source layer within the AAD comes from comparing anomaly widths (Fig. 12a) and seafloor morphology (Fig. 12b) in the eastern AAD (Christie *et al.* 1998; Okino *et al.* 2004). Spreading segments B3w, B5e and B5w, all have typical abyssal hill seafloor fabric approximately perpendicular to the spreading direction and presumably have at least a thin volcanic layer. In contrast, segments B3e and B4 have chaotic seafloor morphology, where long-lived faults may expose the lower crust and upper mantle and the volcanic layer is disturbed and possibly missing. Despite these obvious morphologic differences, the width of Anomaly 1n is nearly identical for all five of these segments.

The Reykjanes ridge has the highest outward displacement in our data set, over 5 km (Fig. 6d). Given the shallow water depths and robust magma supply that characterize much of this hotspot-influenced ridge, a magnetic source model that is dominated by flows travelling far from the axis is more plausible than for the AAD,

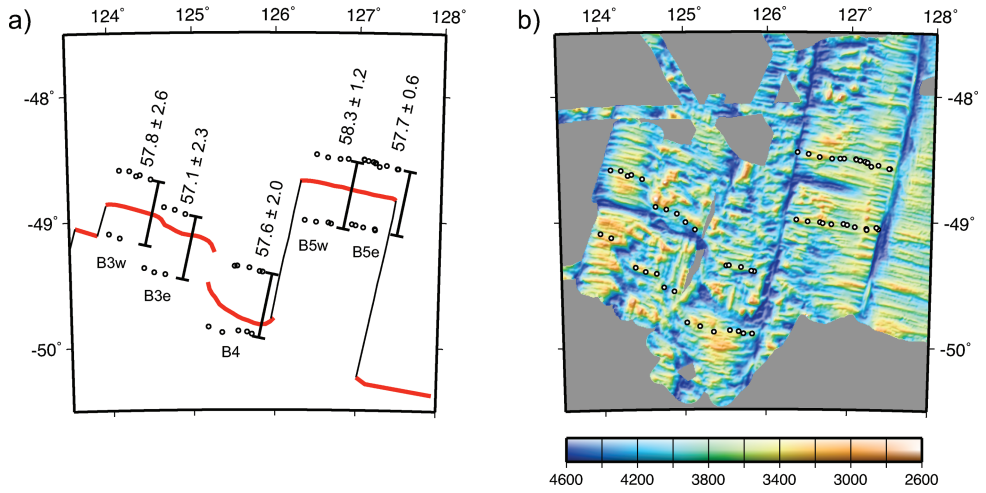

Figure 12. Digitized C1n(o) isochron positions (circles) plotted relative to interpreted plate boundary geometry (a) and multibeam bathymetry (b) for the eastern Australia–Antarctic discordance. Panel (a) shows anomaly widths in kilometres from Fig. 9, with 95 per cent confidence intervals and only isochron picks used in those estimates. Panel (b) shows all C1n(o) isochron picks. The width of C1n(o) is consistently greater than the 55 km width, which is predicted from axial rise segments (Fig. 9) and is fairly uniform between the normal abyssal hill segments B3w, B5w and B5e and the chaotic segments B3e and B4, supporting the interpretation that lavas and upper dykes do not dominate the anomaly source layer here (Fig. 11). Most magnetic and bathymetric data are from cruises KH01-3 (Okino *et al.* 2004) and BMRG05MV (Christie *et al.* 1998).

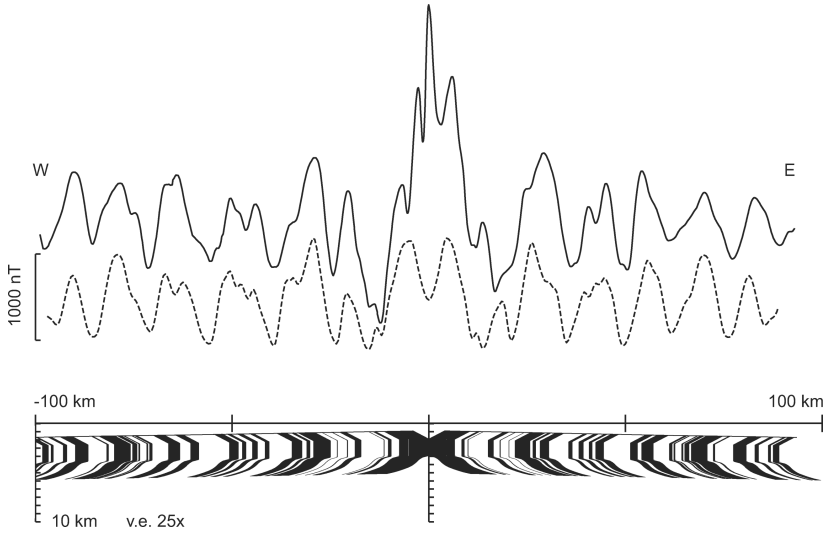

Figure 13. Observed (deskewed) and synthetic magnetic anomalies from the Reykjanes ridge at 61°N. Source model includes a flow layer with magnetization of 4 A m^{-1} and thickness of 1 km forming 0–4 km from the axis, a dyke layer with 1 A m^{-1} magnetization and 2 km thickness and a gabbro layer with 1 A m^{-1} and 2.2-km thickness. Because of shallow water-depth, the calculated anomaly has very large amplitude and is dominated by the flow layer; variations in the lower layers produce only minor changes. Crustal accretion since 6.5 Ma is modelled using rates of 10.7 and 8.5 mm yr^{-1} west and east of the ridge, respectively (19.2 mm yr^{-1} full rate), and a full symmetric rate of 20 mm yr^{-1} prior to 6.5 Ma. NGDC cruise ID is BA75G. No effort has been made to model the magnetic high at the centre of Anomaly 1, thereby accounting for the poor fit to this feature.

where outward displacement is nearly as large. Fig. 13 compares a magnetic anomaly profile that crosses the ridge axis at 61°N to a synthetic profile that is based on a 1-km-thick flow layer, which is assumed to accumulate within 4 km of the ridge axis. Given water depths that are shallower than 1 km, the highly magnetized, outward-sloping upper magnetic layers (flows) strongly influence the magnetic anomalies at the water surface and displace the reversal boundaries outwards from their idealized locations by a distance slightly greater than the transition width. The same geometric effect, whereby the uppermost magnetized layers contribute significantly to the magnetic anomaly that is estimated at the ocean surface, also preserves the short wavelength features in the synthetic profile, which would otherwise not be present at such slow spreading rates ($\sim$18 mm yr^{-1}) if the magnetic polarity transitions were assumed to be distributed uniformly with depth throughout the magnetic source layer.

Although our models for the magnetic source layers in these regions are non-unique, they nonetheless demonstrate that plausible modifications to an idealized 500-m-thick one-layer magnetic source model yield synthetic magnetic profiles that closely match the character of the observed profiles and their observed outward displacement. The characteristics of the magnetic source layers that we employ to achieve the improved fits described above are consistent with those reported by numerous previous authors.

4.3 Implications for models of recent plate motions

Our work has useful implications for both the accuracy and precision of plate motion models that are derived by reconstructing seafloor spreading magnetic lineations. Given the high likelihood that outward displacement occurs everywhere along the mid-ocean ridge system, estimates of seafloor spreading rates that do not correct for outward displacement will systematically overestimate seafloor spreading rates. For example, seafloor spreading rates, which are determined by averaging over the width of Anomaly 1 (781 000 yr), will be too fast by 2.6 mm yr^{-1} at locations where outward displacement equals the global average of 2 km and by 6.4 mm yr^{-1} in areas such as the Reykjanes Ridge where outward displacement is $\sim$5 km. Similarly, for rates that are averaged out to Anomaly 2A (3.16 Ma), as is the case for the NUVEL-1 and NUVEL-1A models, the corresponding rate biases are 0.6 and 1.6 mm yr^{-1} for outward displacement of 2 and 5 km, respectively. These systematic biases are comparable in magnitude to the $\pm$0.7–2 mm yr^{-1} formal uncertainties in the plate rates predicted by NUVEL-1 and NUVEL-1A, neither of which incorporates a correction for outward displacement (DeMets *et al.* 1990, 1994). By implication, both models systematically overestimate present seafloor spreading rates and understate their true prediction errors.

The importance of correcting long-term seafloor opening rates for the effect of outward displacement is well illustrated by a comparison of geological and GPS estimates of the rate of seafloor spreading along the Reykjanes Ridge. From our Reykjanes Ridge age-distance sequence for 60.1°N, 29.3°W (Table 2), we estimate a long-term spreading rate of 21.1 $\pm$ 0.1 mm yr^{-1} if we ignore outward displacement, but a slower rate of 19.2 $\pm$ 0.1 mm yr^{-1} if we correct for outward displacement. At the same location, two recently published GPS-based models based on the velocities of numerous continuous GPS stations from the North American and Eurasian plates predict opening rates of 19.8 $\pm$ 0.2 and 19.6 mm yr^{-1} (Calais *et al.* 2003 and the GSRM v1.2 model of Kreemer *et al.* 2003). Both GPS rates agree significantly better with the 19.2 $\pm$ 0.1 mm yr^{-1} seafloor spreading rate, which is corrected for outward displacement, than they do with the uncorrected long-term rate of 21.1 $\pm$ 0.1 mm yr^{-1} and are consistent with a simple model in which the Reykjanes Ridge spreading rate has remained constant for the past several million years.

Ideally, future plate motion models that are based wholly or partly on marine magnetic data will incorporate corrections for outward displacement that vary by location and are based on analyses such as this. Location-specific corrections are presently feasible for densely

surveyed plate boundaries such as Eurasia–North America, Africa–North America, the Southeast Indian Ridge and the Carlsberg Ridge. These, however, are the exception. Along the 30 per cent of the mid-ocean ridge system where ultra-slow spreading occurs, no estimate of outward displacement is available due to the poor fidelity with which magnetic anomaly sequences are recorded at such slow spreading rates. In addition, few constraints exist for the magnitude of outward displacement along fast seafloor spreading centres because most fast seafloor spreading centres are located in the Pacific basin, where opening rates have changed along all but one spreading centre in the past few million years.

Our analysis indicates that to first order, outward displacement at most locations is consistent with a global average value of 2.2 ± 0.3 km. Correcting most or all seafloor spreading rates using this average value for outward displacement would thus eliminate most of the systematic bias in rates that are estimated at most locations. Along the fast seafloor spreading centres in the Pacific basin, where we have the fewest constraints, inversions of near-bottom magnetic profiles across the 150 mm yr^{-1} spreading East Pacific Rise at 20°S yield polarity zone transition widths of 1.7 km (Sempere *et al.* 1987). This is encouragingly close to the global average that we estimate and suggests that a ∼2 km correction for outward displacement is approximately correct for fast seafloor spreading rates.

ACKNOWLEDGMENTS

We thank S. Cande, L. Geli, P. Gente and K. Okino for providing magnetic and multibeam data and S. Cande and J. Dyment for helpful reviews. This work was funded by NSF grants OCE-9902818 and OCE-0453113. Figures were produced using Generic Mapping Tools software (Wessel & Smith 1991).

REFERENCES

Anderson, R.N., Spariosu, D.J., Weissel, J.K. & Hayes, D.E., 1980. The interrelation between variations in magnetic anomaly amplitudes and basalt magnetization and chemistry along the Southeast Indian ridge, *J. geophys. Res.,* **85,** 3883–3898.

Argus, D.F., 2007. Defining the translational velocity of the reference frame of Earth, *Geophys. J. Int.,* **169,** 830–838, doi:10.1111j.1365-246X.2007.03344.x.

Argus, D.F., Gordon, R.G., DeMets, C. & Stein, S., 1989. Closure of the Africa-Eurasia-North America plate motion circuit and tectonics of the Gloria fault, *J. geophys. Res.,* **94,** 5585–5602.

Argus, D.F., Peltier, W.R. & Watkins, M.M., 1999. Glacial isostatic adjustment observed using very long baseline interferometry and satellite laser ranging geodesy, *J. geophys. Res.,* **104,** 29 077–29 093.

Arkani-Hamed, J., 1989. Thermo-viscous remanent magnetization of oceanic lithosphere inferred from its thermal evolution, *J. geophys. Res.,* **94,** 17 421–17 436.

Atwater, T. & Mudie, J.D., 1973. Detailed near-bottom geophysical study of the Gorda Rise, *J. geophys. Res.,* **78,** 8665–8686.

Blakely, R.J., 1976. An age dependent, two layer model for marine magnetic anomalies, in *The Geophysics of the Pacific Ocean Basin and Its Margin, Geophys. Monogr. Ser.*, Vol. 19, pp. 227–234, eds Sutton, G.H., Manghnani, M.H., Moberly, R. & McAfee, E.U., Am. Geophys. Un., Washington, DC.

Blakely, R.J. & Lynn, W.S., 1977. Reversal transition widths and fast-spreading centers, *Earth planet. Sci. Lett.,* **33,** 321–330.

Blewitt, G., 2003. Self-consistency in reference frames, geocenter definition, and surface loading of the solid Earth, *J. geophys. Res.,* **108,** doi:10.10292002JB002082.

Calais, E., DeMets, C. & Nocquet, J.-M., 2003. Evidence for a post-3.16 Ma change in Nubia-Eurasia-North America plate motions?, *Earth planet. Sci. Lett.,* **216,** 81–92.

Cande, S.C. & Kent, D.V., 1976. Constraints imposed by the shape of marine magnetic anomalies on the magnetic source, *J. geophys. Res.,* **81,** 4157–4162.

Cande, S.C. & Kent, D.V., 1992. A new geomagnetic polarity time scale for the Late Cretaceous and Cenozoic, *J. geophys. Res.,* **97,** 13 917–13 951.

Christie, D.M., West, B.P., Pyle, D.G. & Hanan, B.A., 1998. Chaotic topography, mantle flow, and mantle migration in the Australia-Antarctic discordance, *Nature,* **394,** 637–644.

Chu, D. & Gordon, R.G., 1999. Evidence for motion between Nubia and Somalia along the Southwest Indian Ridge, *Nature,* **398,** 64–67.

Cochran, J.R., Sempere, J.-C. & SEIR Scientific Team, 1997. The Southeast Indian Ridge between 88°E and 118°E: gravity anomalies and crustal accretion at intermediate spreading rates, *J. geophys. Res.,* **102,** 15 463–15 487.

DeMets, C., 1993. Earthquake slip vectors and estimates of present-day plate motions, *J. geophys. Res.,* **98,** 6703–6714.

DeMets, C. & Traylen, S., 2000. Motion of the Rivera plate since 10 Ma relative to the Pacific and North American plates and the mantle, *Tectonophysics,* **318,** 119–159.

DeMets, C. & Wilson, D.S., 1997. Relative motions of the Pacific, Rivera, North American, and Cocos plates since 0.78 Ma, *J. geophys. Res.,* **102,** 2789–2806.

DeMets, C., Gordon, R.G., Argus, D.F. & Stein, S., 1990. Current plate motions, *Geophys. J. Int.,* **101,** 425–478.

DeMets, C., Gordon, R.G., Argus, D.F. & Stein, S., 1994. Effect of recent revisions to the geomagnetic reversal timescale on estimates of current plate motions, *Geophys. Res. Lett.,* **21,** 2191–2194.

DeMets, C., Gordon, R.G. & Royer, J.-Y., 2005. Motion between the Indian, Capricorn, and Somalian plates since 20 Ma: implications for the timing and magnitude of distributed deformation in the equatorial Indian ocean, *Geophys. J. Int.,* **161,** 445–468.

Dixon, T. *et al.*, 2000. New kinematic models for Pacific-North America motion from 3 Ma to present, II: tectonic implications for Baja and Alta California, *Geophys. Res. Lett.,* **27,** 3961–3964.

Dyment, J. & Arkani-Hamed, J., 1995. Spreading-rate-dependent magnetization of the oceanic lithosphere inferred from the anomalous skewness of marine magnetic anomalies, *Geophys. J. Int.,* **121,** 789–804.

Dyment, J., Arkani-Hamed, J. & Ghods, A., 1997. Contribution of serpentinized ultramafics to marine magnetic anomalies at slow and intermediate spreading centres: insights from the shape of the anomalies, *Geophys. J. Int.,* **129,** 691–701.

Gee, J. & Kent, D.V., 1998. Magnetic telechemistry and magmatic segmentation on the southern East Pacific Rise, *Earth planet. Sci. Lett.,* **164,** 379–385.

Hellinger, S.J., 1979. The statistics of finite rotations in plate tectonics, unpublished *PhD thesis*, Massachusetts Institute of Technology, MA, 172 pp.

Jarrard, R.D., 1986. Terrane motion by strike-slip faulting of forearc slivers *Geology,* **14,** 780–783.

Kidd, R.G.W., 1977. A model for the process of formation of the upper oceanic crust, *Geophys. J. R. astr. Soc.,* **50,** 149–183.

Klitgord, K.D., Heustis, S.P., Mudie, J.D. & Parker, R.L., 1975. An analysis of near-bottom magnetic anomalies: seafloor spreading and the magnetized layer, *Geophys. J. R. astr. Soc.,* **43,** 387–424.

Kojima, Y., Shinohara, M., Mochizuki, K., Yamada, T., Nakahigashi, K. & Kanazawa, T., 2003. Seismic velocity structure in the Australian-Antarctic discordance, Segment B4 revealed by airgun-OBS experiment (abstract), *EOS, Trans. Am. geophys. Un.,* **84**(46), S21F0396K.

Kreemer, C., Holt, W.E. & Haines, A.J., 2003. An integrated global model of present-day plate motions and plate boundary deformation, *Geophys. J. Int.,* **154,** 8–34.

Krijgsman, W., Hilgen, F.J., Raffi, I., Sierro, F.J. & Wilson, D.S., 1999. Chronology, causes, and progression of the Messinian salinity crisis, *Nature,* **400,** 652–655.

Larson, K.M., Freymueller, J.T. & Philipsen, S., 1997. Global plate velocities from the Global Positioning System, *J. geophys. Res.,* **102,** 9962–9982.

Lourens, L., Hilgen, F.J., Laskar, J., Shackleton, N.J. & Wilson, D., 2004. The Neogene Period, in *A Geologic Time Scale 2004*, pp. 409–440, eds Gradstein, F., Ogg, J. & Smith, A., Cambridge University Press, London.

Macdonald, K.C., 1977. Near bottom magnetic anomalies, asymmetric spreading, oblique spreading and tectonics of the Mid-Atlantic Ridge near Lat 37°N, *Geol. Soc. Am. Bull.,* **88,** 541–555.

Macdonald, K.C., Miller, S.P., Huestis, S.P. & Spiess, F.N., 1980. Three-dimensional modeling of a magnetic reversal boundary from inversion of deep-tow measurements, *J. geophys. Res.,* **85,** 3670–3680.

Macdonald, K.C., Miller, S.P., Luyendyk, B.P., Atwater, T.M. & Shure, L., 1983. Investigation of a Vine-Matthews magnetic lineation from a submersible: the source and character of marine magnetic anomalies, *J. geophys. Res.,* **88,** 3403–3418.

Macdonald, K.C. et al., 1992. The East Pacific Rise and its flanks 8–18°N: history of segmentation, propagation and spreading direction based on SeaMARC II and Sea Beam studies, *Mar. Geophys. Res.,* **14,** 299–344.

McCaffrey, R., 1992. Oblique plate convergence, slip vectors, and forearc deformation, *J. geophys. Res.,* **97,** 8905–8915.

Merkouriev, S. & DeMets, C., 2006. Constraints on Indian plate motion since 20 Ma from dense Russian magnetic data: implications for Indian plate dynamics, *Geochem. Geophys. Geosyst.,* **7,** Q02002, doi:10.1029/2005GC001079.

Merkouriev, S. & DeMets, C., 2008. A high-resolution model for Eurasia-North America plate kinematics since 20 Ma, *Geophys. J. Int.,* **173,** 1064–1083.

Minster, J.B. & Jordan, T.H., 1978. Present-day plate motions *J. geophys. Res.,* **83,** 5331–5354.

Naar, D.F. & Hey, R.N., 1989. Recent Pacific-Easter-Nazca plate motions, in *Evolution of Mid Ocean Ridges*, Vol. 57, pp. 9–30, ed. Sinton, J.M., Am. Geophys. Un. Geophysical Monograph series.

Okino, K., Matsuda, K., Christie, D.M., Nogi, Y. & and Koizumi, K., 2004. Development of oceanic detachment and asymmetric spreading at the Australia-Antarctic Discordance, *Geochem. Geophys. Geosys.,* **5**(12), Q12012, doi:10.1029/2004GC000793.

Plattner, C., Malservisi, R., Dixon, T.H., LaFemina, P., Sella, G., Fletcher, J. & Suarez-Vidal, F., 2007. New constraints on relative motion between the Pacific plate and Baja California microplate (Mexico) from GPS measurements, *Geophys. J. Int.,* **170,** 1373–1380, doi:10.1111j.1365–246X.2007.03494.x.

Royer, J.-Y. & Chang, T., 1991. Evidence for relative motions between the Indian and Australian plates during the last 20 Myr from plate tectonic reconstructions: implications for the deformation of the Indo-Australian plate, *J. geophys. Res.,* **96,** 11 779–11 802.

Royer, J.-Y., Gordon, R.G. & Horner-Johnson, B.C., 2006. Motion of Nubia relative to Antarctica since 11 Ma: implications for Nubia-Somalia, Pacific-North America, and India-Eurasia motion, *Geology,* **34,** 501–504, doi:10.1130G22463.1.

Sandwell, D.T. & Smith, W.H.F., 1997. Marine gravity anomaly from Geosat and ERS1 altimetry, *J. geophys. Res.,* **102,** 10 039–10 054.

Schouten, H. & Denham, C.R., 1979. Modeling the oceanic magnetic source layer, in *Deep Drilling Results in the Atlantic Ocean: Ocean Crust, Maurice Ewing Series*, Vol. 2, pp. 151–159, eds Talwani, M., Harrison, C.G. & Hayes, D.E., Am. Geophys. Union, Washington, DC.

Sella, G.F., Dixon, T.H. & Mao, A., 2002. REVEL: a model for recent plate velocities from space geodesy, *J. geophys. Res.,* **107**(B4), doi:10.1029/2000JB000033.

Sempere, J.-C., Macdonald, K.C. & Miller, S.P., 1987. Detailed study of the Brunhes/Matuyama reversal boundary on the East Pacific Rise at 19°30′ S: implications for crustal emplacement processes at an ultra fast spreading center, *Mar. Geophys. Res.,* **9,** 1–23.

Sempere, J.-C., Kristjansson, L., Schouten, H., Heirtzler, J.R. & Johnson, G.L., 1990. A detailed magnetic study of the Reykjanes Ridge between 63°00′N and 63° 40′N, *Mar. Geophys. Res.,* **12,** 215–234.

Tebbens, S.F., Cande, S.C., Kovacs, L., Parra, J.C., LaBrecque, J.L. & Vergara, H., 1997. The Chile Ridge: a tectonic framework, *J. geophys. Res.,* **102,** 12 035–12 059.

Tivey, M.A., Johnson, H.P., Fleutelot, C., Hussenoeder, S., Lawrence, R., Waters, C. & Wooding, B., 1998. Direct measurement of magnetic reversal polarity boundaries in a cross-section of oceanic crust, *Geophys. Res. Lett.,* **25,** 3631–3634.

Tolstoy, M., Harding, A.J., Orcutt, J.A. & Phipps-Morgan, J., 1995. Crustal thickness at the Australian-Antarctic discordance and neighboring Southeast Indian Ridge (abstract), *EOS, Trans. Am. geophys. Un.,* **76**(46), F570.

Vine, F.J. & Matthews, D.H., 1963. Magnetic anomalies over oceanic ridges, *Nature,* **199,** 947–949.

Vogt, P.R. & Johnson, G.L., 1973. Magnetic telechemistry of oceanic crust?, *Nature,* **245,** 373–375.

Weiland, C., Wilson, D.S. & Macdonald, K., 1995. High-resolution plate reconstruction of the southern Mid-Atlantic ridge, *Mar. Geophys. Res.,* **17,** 143–166.

Weissel, J.K. & Hayes, D.E., 1974. The Australian-Antarctic discordance: new results and implications, *J. geophys. Res.,* **79,** 2579–2587.

Wessel, P. & Smith, W.H.F., 1991. Free software helps map and display data, *EOS, Trans. Am. geophys. Un.,* **72,** 441–446.

Wilson, D.S., 1993a. Confidence intervals for motion and deformation of the Juan de Fuca plate, *J. geophys. Res.,* **98,** 16 053–16 071.

Wilson, D.S., 1993b. Confirmation of the astronomical calibration of the magnetic polarity timescale from sea-floor spreading rates, *Nature,* **364,** 788–790.

Wilson, D.S. & Hey, R.N., 1995. History of rift propagation and magnetization intensity for the Cocos-Nazca spreading center, *J. geophys. Res.,* **100,** 10 041–10 056.